Ergodic characterization of nonergodic anomalous diffusion processes

Madhur Mangalam [*]
Division of Biomechanics and Research Development, Department of Biomechanics, and Center for Research in Human Movement Variability, University of Nebraska at Omaha, Omaha, Nebraska 68182, USA

Ralf Metzler
Institute of Physics & Astronomy, University of Potsdam, 14776 Potsdam, Germany

Damian G. Kelty-Stephen
Department of Psychology, State University of New York at New Paltz, New Paltz, New York 12561, USA

(Received 9 February 2023; accepted 8 May 2023; published 31 May 2023)

Anomalous diffusion in various complex systems abounds in nature and spans multiple space and time scales. Canonical characterization techniques that rely upon mean squared displacement break down for nonergodic processes, making it challenging to characterize anomalous diffusion from an individual time-series measurement. Nonergodicity reigns when the time-averaged mean square displacement differs from the ensemble-averaged mean squared displacement even in the limit of long measurement series. In these cases, the typical theoretical results for ensemble averages cannot be used to understand and interpret data acquired from time averages. The difficulty then lies in obtaining statistical descriptors of the measured diffusion process that are not nonergodic. We show that linear descriptors such as the standard deviation, coefficient of variation, and root mean square break ergodicity in proportion to nonergodicity in the diffusion process. In contrast, time series of descriptors addressing sequential structure and its potential nonlinearity: multifractality change in a time-independent way and fulfill the ergodic assumption, largely independent of the time series' nonergodicity. We show that these findings follow the multiplicative cascades underlying these diffusion processes. Adding fractal and multifractal descriptors to typical linear descriptors would improve the characterization of anomalous diffusion processes. Two particular points bear emphasis here. First, as an appropriate formalism for encoding the nonlinearity that might generate nonergodicity, multifractal modeling offers descriptors that can behave ergodically enough to meet the needs of linear modeling. Second, this capacity to describe nonergodic processes in ergodic terms offers the possibility that multifractal modeling could unify several disparate nonergodic diffusion processes into a common framework.

DOI: 10.1103/PhysRevResearch.5.023144

I. INTRODUCTION

Anomalous diffusion abounds in nature—atoms in magneto-optical traps [1,2], DNA, lipids, and proteins [3–12], bacteria, cells, and parasites [13–19], foraging wild animals [20–22] and human hunter gatherers [23,24], economic markets [25–27], and various other processes [28–31] show anomalous diffusion that spans multiple scales [Fig. 1(a)]. All these processes are characterized by an erratic change of an observable (e.g., position, temperature, or stock price) over time [Fig. 1(b)]. "Anomalous" implies that the observable x's mean squared displacement (MSD) does not grow linearly with time t, $\langle x^2(t)\rangle \propto t$, as predicted by Fick's theory of diffusion, but follows another power-law pattern $\langle x^2(t)\rangle \propto t^\alpha$, with $\alpha \neq 1$. Notably, exceptions exist, and the time evolution of anomalous diffusion regimes' MSD does not always follow a power-law form (e.g., Sinai diffusion [32–34]). Frequently, $\alpha < 1$, indicating subdiffusion [16,35–41]. Superdiffusion—characterized by $\alpha > 1$—is less commonly reported than subdiffusion but is often observed in active physical and biological systems [36,42–49].

Widespread evidence of anomalous diffusion processes has sparked a major theoretical effort to comprehend and formally organize the mechanisms that might explain them. This endeavor has resulted in various mathematical models with and without long-range correlations and varied spatial (step length) and temporal (step duration) random distributions. Models of anomalous diffusion have grown from elaborations of Brownian motion, which depicts the movement of a small particle in a fluid due to thermal forces. Brownian motion embodies ordinary diffusion when MSD grows linearly with time, $\langle x^2(t)\rangle \propto t$ [51]. In a curious turn of terminology, anomalous diffusion emerges as the more general case—"anomalous is normal" [52], and these widespread applications of diffusion modeling come from adding an anomalous nuance to these fluctuation patterns in the narrow

[*]Author to whom correspondence should be addressed: mmangalam@uomaha.edu

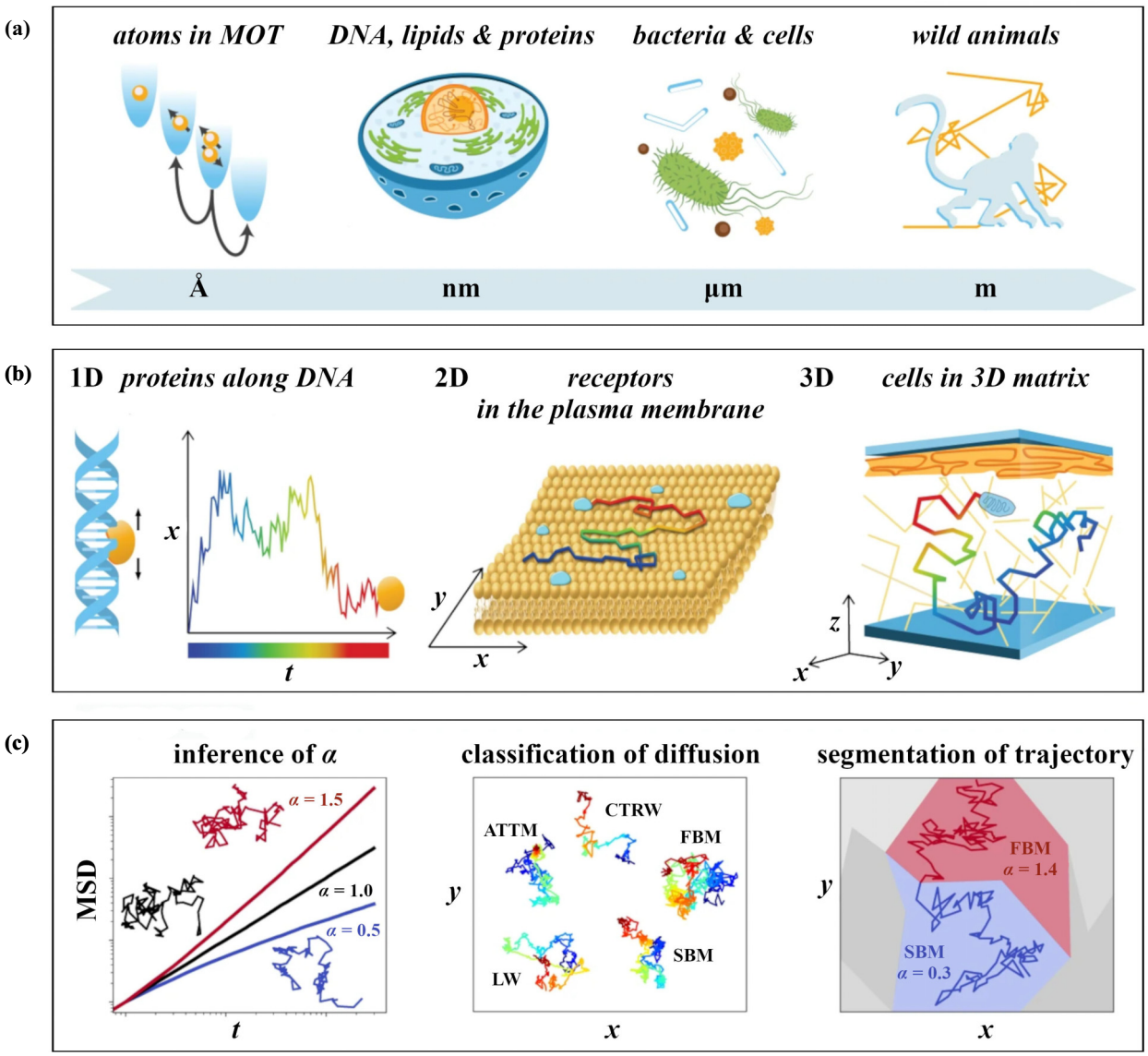

FIG. 1. Random walks or anomalous diffusion processes, defined by unpredictable variations in an observable, can be found in various systems over a wide range of spatial and temporal scales. (a) Examples include atoms in magneto-optical traps, the diffusion of biological components such as DNA, lipids, and proteins, bacteria and cell motility, and foraging wild animals. (b) Random walks in three-dimensional spaces may be dimensionally reduced: 1D, proteins sliding along DNA segments; 2D, receptors diffusing across the plasma membrane; 3D, cells migrating through a three-dimensional matrix. The color code of the trajectories represents time. (c) Representative trajectories and corresponding MSD for diffusive ($\alpha = 1$, black lines), subdiffusive ($0 < \alpha < 1$, blue lines), and superdiffusive ($1 < \alpha < 2$, red lines) motion. The underlying anomalous diffusion model can be classified as fractional Brownian motion, scaled Brownian motion, continuous time random walk, annealed transient time motion, or Lévy walk. These diffusion models produce subtle changes. A trajectory can show a change point by switching the diffusion model or exponent due to diffusion in a spatially heterogeneous environment. Adapted from Muñoz-Gil *et al.* [50].

case of so-called "ordinary" diffusion [52]. The anomalous diffusion underlying an observed process can be modeled as fractional Brownian motion (FBM) [53], scaled Brownian motion (SBM) [54,55], noisy continuous time random walk (nCTRW)—a variant of CTRW with the power-law distribution of waiting times [55–57], annealed transient time motion (ATTM) [58], or Lévy walk (LW) [59]. These diffusion processes show subtle differences in how fluctuations are distributed in time (for details of the models, see Appendix A). Indeed, the problem of ergodicity breaking also arises for other types of diffusion anomalies [60]. The theoretical challenge for explaining anomalous diffusion compounds with the observation that these different processes are not mutually exclusive—they may only reflect distinct modes into which the same observable system can transition [50,61]. A single observed trajectory can switch at change points among regimes best explained by different of these models as a result of interactions with the surroundings in a heterogeneous environment [3,7,8,62–65] [Fig. 1(c)]. The observed motion often simultaneously exhibits features of more than one of the "elementary" stochastic models. Despite their common heritage in Brownian motion [66], these processes exhibit seemingly disparate modes of nonlinear and nonergodic behavior [52,65,67–70]. The challenge is that modeling the

causal evolution from one mode to another requires causal models, and prevailing statistical approaches to causal modeling largely assume linearity and ergodicity.

A leading motivation to study anomalous diffusion models is to detect and classify specific anomalous diffusion processes in empirical data. However, all the above factors make this classification a challenging feat. Therefore, recent attempts include Bayesian [71–75] as well as machine-learning (ML) approaches [50,76–80], and even unsupervised approaches [81–86]. However, these attempts are based on an atheoretical selection of features which may not necessarily be related to plausible generating mechanisms [87,88]. A more theoretically defined set of features can potentially improve the ML-powered characterization of anomalous diffusion processes in empirical data.

One possible resolution lies in the observation that temporal correlations and non-Gaussianity are common features of multifractal processes. Multifractal geometry is also a formalism that specifically addresses the intermittent, nonergodic fluctuations across a wide range of scales and the nonlinear interactions of short-range events with large-scale contextual factors [89,90]. Multifractality is observed in strong anomalous diffusion [91,92]. Thus, these anomalous processes with common heritage in the Brownian-motion formalism may find a common reunified description. This point is not to say that the models generating these different regimes of anomalous diffusion are explicitly multifractal. Instead, it is to recognize that multifractal geometry has long been considered a modeling framework broad enough to explain how these modes of anomalous diffusion evolve over time and sometimes with change points from one mode to another [93]. Critically, the first step towards explanation through prevailing causal models is meeting the basic benchmark of ergodicity for the traditionally linear statistical structure of causal modeling. We use numerical simulations to test the hypothesis that multifractal geometrical estimates of these diffusive properties offer an ergodic descriptor that makes these disparate diffusion processes amenable to a linear causal framework.

Efforts so far have addressed the twofold challenges of properly quantifying empirical diffusion processes and doing so with the appropriate model. The difficulty here is that both concerns must be pursued largely in tandem: we must empirically estimate the value of model parameters, and to ensure these estimates are effective, we must be sure to use a model appropriate to the data. Best practices for balancing parameter estimation with model specification includes analyzing the empirical time-series data with various statistical observables such as MSD, spectral power analysis, van Hove correlation functions, step-length or flight-time distribution, and ergodicity-breaking parameter [31,94–103]. However, data interpretation can be subjective and is contingent on the fidelity of the observed data which is inevitably constrained by length and number of observations, measurement noise, and sample spatiotemporal heterogeneity.

It is important to note that the preceding best practices are sometimes at odds with the characteristic nonergodicity of many anomalous-diffusion processes. That is to say, the constraints imposed by ergodicity on diffusion modeling set in well before any thoughts about linear causal models to articulate any causal developmental relationships among disparate anomalous-diffusion processes. Nonergodicity entails a failure of individual time-series measurements to represent an ensemble. Nonergodicity reigns when time-averaged MSD (TA-MSD) differs from ensemble-averaged MSD (EA-MSD). Sample-size constraints on measurements of nonergodic processes thus dramatically constrain the interpretation of the canonical characterization techniques that rely on MSD. In these cases, the typical theoretical results for ensemble averages cannot be used to understand and interpret data acquired from time averages. For example, FBM is ergodic for $\alpha = 0.1$, although convergence of the EA-MSD to TA-MSD may be slower for values of the anomalous exponent close to 1 [104]. The ergodicity in FBM requires careful analysis as a function of α [105–108], and often higher-order moments accounting for the skewness and kurtosis are necessary to study ergodicity breaking in FBM [109]. CTRW, ATTM, and SBM show weak ergodicity breaking [7,58,92,110–113]. Finally, a LW shows a distinct kind of ergodicity breaking—named ultraweak nonergodicity—in which ensemble and time averages only differ by a constant factor [114,115]. Deriving inferences from canonical estimates submitted to linear causal models makes the questionable compromise of enforcing similarity while neglecting diversity for formal convenience, given the variability in the ergodic features of these diffusion processes. Moreover, such inferences may obscure any artifacts of nonergodicity or fail to articulate the systematic changes that lead to nonergodicity, potentially obscuring any genuine individual differences and discarding any generalizable truths we might have gleaned from the same diversity that was intended to represent these disparate models of nonlinearity and nonergodicity [107].

Here, we have used cascade-dynamical descriptors rooted in multifractal formalism to compare the ergodicity-related diffusive properties of various anomalous processes. An important theoretical move beyond attempts at formal convenience may be explicitly addressing the underlying mechanisms generating nonergodicity in empirical examples of anomalous diffusion. In this sense, multifractal geometry is not merely convenient because it affords an analytical repertoire for addressing features sometimes seen in different anomalous-diffusion processes. Rather, multifractal geometry is a theoretically valid means to estimate parameters of cascade dynamics that can generate a wide variety of intermittent, nonergodic behavior. If we encode those aspects of the diffusion process known to generate nonergodicity, these parameter estimates might be ergodic—and indeed, current evidence shows that they are [105,108]. We know, for instance, that fGn observed in biological and psychological phenomena break ergodicity primarily due to the interdependencies among factors unfolding at multiple spatial and temporal scales [116–120]. The scale-invariant shape of the power-law autocorrelation in fGn—quantified as the fractal exponent H_{fGn} shows none of the ergodicity breaking of the fGn series [108,108]. Although fGn is a linear process, one possible explanation for power-law scaling is the nonlinear interactions across scales in cascade processes known to generate intermittent, nonergodic behavior [89]. The strength of cascade dynamics can be quantified as the multifractal spectrum width $\Delta\alpha$ and then as a t-statistic comparing that multifractal-spectrum width to spectrum widths for linear

surrogates t_{MF} [121,122]. If cascades can explain the nonergodic behavior of all anomalous diffusion processes, then $\Delta\alpha$ and t_{MF} might avoid displaying the breaking of ergodicity and can be submitted to linear models of cause and effect. Indeed, we have shown that for fGn, all three descriptors: H_{fGn}, $\Delta\alpha$, and t_{MF}, avoid ergodicity breaking [105,108]. Even without any interest in causal modeling to examine the developmental change among modes of anomalous diffusion, this approach of extending beyond MSD to more generalized multifractal modeling can help restore broken ergodicity for all forms of anomalous diffusion processes.

The structure of this article is as follows: We first provide a comparative analysis of the ergodic properties of synthetic FBM, SBM, nCTRW, ATTM, and LW time series with different values of the anomalous exponent. We then provide a comparative analysis of the ergodic properties of the time series of linear and cascade-dynamical descriptors of these synthetic time series. We discuss how the latter descriptors—rooted in multifractal formalism—encode the nonlinearity that might generate nonergodicity in these anomalous diffusion processes. Finally, we discuss the implications of using cascade-dynamical descriptors of anomalous diffusion processes to meet the needs of linear modeling and classify specific anomalous diffusion processes in empirical data.

II. MATERIALS AND METHODS

A. Simulating FBM, SBM, nCTRW, ATTM, and LW series

We simulated using MATLAB (Matlab Inc, Natick, MA, USA) 50 001-sample synthetic trajectories generated according to each of the following five different anomalous diffusion models [Fig. 2(a)]: (i) FBM (ergodic)—a motion with correlated long-range steps [53], (ii) SBM (weakly nonergodic)—a motion whose diffusion coefficient features deterministic time-dependent changes [54,55], (iii) nCTRW (weakly nonergodic)—a variant of CTRW [57], a motion undergoing local trapping with a wide distribution of waiting times [56], (iv) ATTM (weakly nonergodic)—a motion with random changes of the diffusion coefficient in time [58], and (iv) LW (ultraweakly nonergodic)—a motion displaying irregular jumps with constant velocity [59]. Appendix A describes the anomalous diffusion models and the algorithm used to simulate each process in more detail. The anomalous exponent was restricted to $\alpha \geqslant 0.1$ because smaller exponents produce practically immobile trajectories. Note that FBM, SBM, nCTRW, and ATTM are considered in the subdiffusive range $0.1 \leqslant \alpha \leqslant 1$, and LW is subdiffusive in the range $\alpha \geqslant 1$. We simulated 100 series using each of the 10 different exponents for each model: $\alpha = \{0.1, 0.2, \ldots, 1\}$ for FBM, SBM, nCTRW, and ATTM, and $\alpha = \{1.1, 1.2, \ldots, 2\}$ for LW. Each series was then differentiated, and its absolute value was taken to obtain a 50 000-sample fluctuation series. All analysis was conducted on these fluctuation series because multifractal analysis requires all values in a time series to be positive. Using absolute values is a common practice in fractal and multifractal analysis. A shuffled version of each original fluctuation series was generated for comparison because ergodicity is about how sequence exemplifies a typical mean trajectory of a sample of realizations. Shuffling breaks the sequence, producing additive white Gaussian noise (awGn) oscillating around the mean. Finally, each original series $x(t)$ was segmented into 100 nonoverlapping 500-sample segments, s, such that $s = \{s_1, s_2, \ldots, s_{100}\}$. The corresponding shuffled version for each process was likewise segmented. 100-sample time series of linear and nonlinear descriptors were obtained across these segmented series. This procedure breaks long-range correlations in the process, as shown below.

B. Estimating linear descriptors

We computed EA-MSD and TA-MSD for each process trajectory. We defined EA-MSD as

$$\langle x^2(t)\rangle = \frac{1}{N}\sum_{i=1}^{N}[x_i(t) - x_i(0)]^2, \tag{1}$$

for a set of N trajectories, and we defined the time-average mean squared displacement (TA-MSD) as

$$\overline{\delta^2(\tau)} = \frac{1}{L-m}\sum_{i=1}^{L-m}\{x[(i+m)\Delta t] - x(i\Delta t)\}^2, \tag{2}$$

when the series is sampled at L discrete times $\tau = m\Delta t$.

We also computed MSD-related three linear descriptors for each of the 100 nonoverlapping 500-sample segments for the original version (i.e., unshuffled) and a shuffled version (i.e., a version with the temporal information destroyed) of each process. We defined the standard deviation (SD) as

$$SD = \sqrt{\frac{1}{T}\sum_{t=1}^{T}(x(t) - \overline{x(t)})^2}, \tag{3}$$

where T is the fluctuation series length, and we defined the coefficient of variation (CV) as

$$CV = \frac{\sqrt{\frac{1}{T}\sum_{t=1}^{T}(x(t) - \overline{x(t)})^2}}{\overline{x(t)}}. \tag{4}$$

We also defined the root mean square (RMS), i.e.,

$$RMS = \sqrt{\frac{1}{T}\sum_{t=1}^{T}|x(t)|^2}. \tag{5}$$

C. Estimating cascade-dynamical descriptors

Previous research has supported the idea that fractal and multifractal estimates offer a more accurate characterization of measurement series that exhibit ergodicity-breaking features such as correlations [108], non-Gaussianity [105], and cascade dynamics [106], compared with conventional linear-modeling estimates of variability. This promising outcome has encouraged further investigation. However, previous work has been limited to explicit models of non-Gaussian, correlated, and cascade-dynamical fluctuations. Therefore, we aimed to test the effectiveness of multifractal estimates in characterizing a wider range of anomalous diffusion models, which may better represent biological motility and offer a more comprehensive understanding of ergodicity. We computed three cascade-dynamical descriptors for each of the 100 nonoverlapping 500-sample segments for the original version (i.e.,

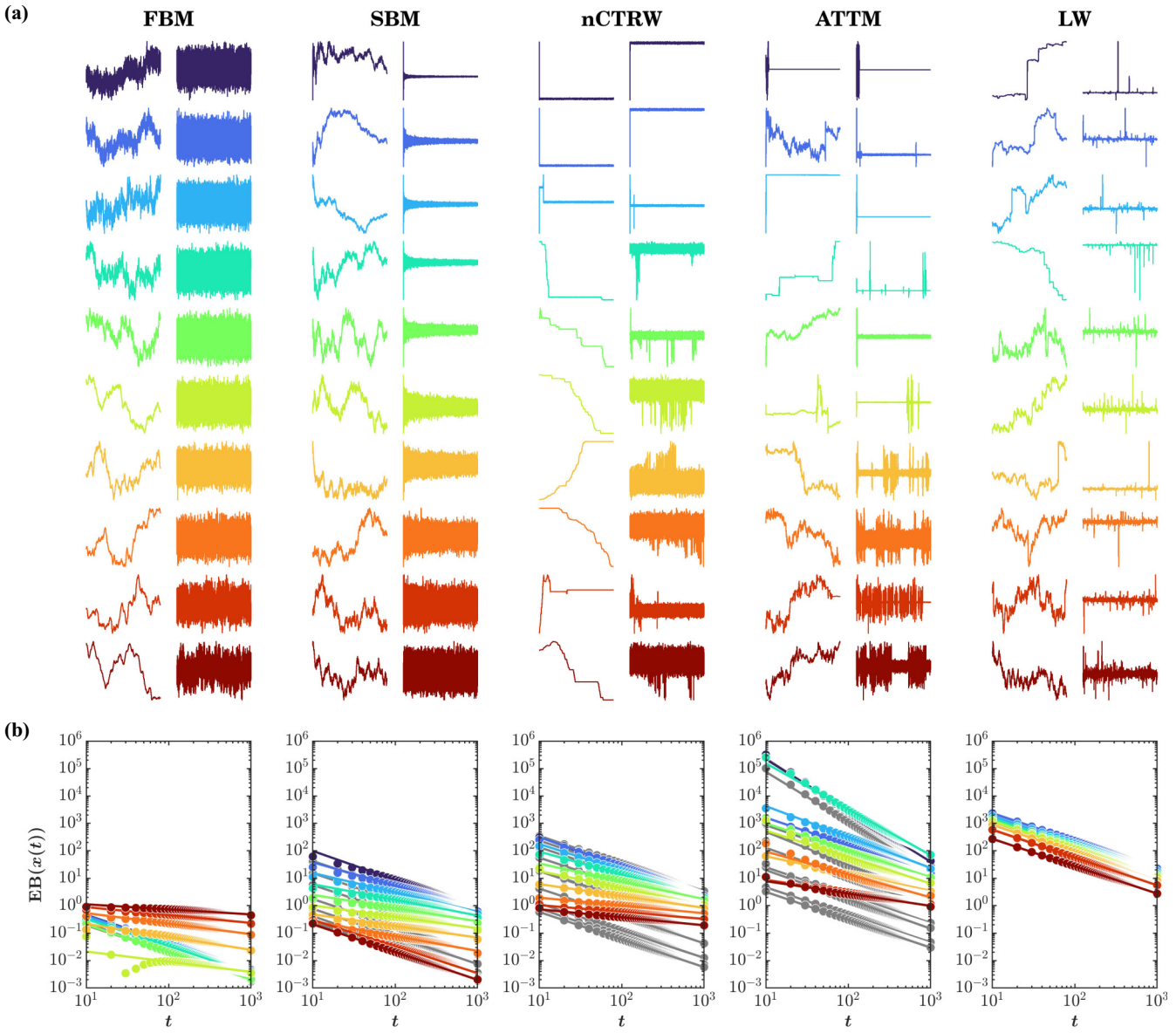

FIG. 2. Simulated anomalous diffusion processes and their ergodic properties. (a) Sample trajectories, and the corresponding fluctuation series, were generated according to the following five models: fractional Brownian motion (FBM, ergodic), scaled Brownian motion (SBM, weakly nonergodic), noisy continuous time random walk (nCTRW, weakly nonergodic), annealed transient time motion (ATTM, weakly nonergodic), and Lévy walk (LW, ultraweakly nonergodic). While FBM, SBM, nCTRW, and ATTM are strictly subdiffusive ($0.1 \leqslant \alpha \leqslant 1$), LW is superdiffusive ($\alpha \geqslant 1$). The anomalous exponent α ranges from 0.1 to 1 for FBM, SBM, nCTRW, and ATTM and from 1.1 to 2 for LW, with an increment of 0.1 from top to bottom. (b) Ergodicity-breaking parameter [EB($x(t)$)] for each of the five processes ($N = 100$; lag is $\Delta = 10$ samples). The different decay rates of EB $\to 0$ as $t \to \infty$ for different diffusion models and exponents indicate that each process breaks ergodicity to different extents: FBM, ergodic; SBM, weakly nonergodic; nCTRW, weakly nonergodic; ATTM, weakly nonergodic; and LW, ultraweakly nonergodic. Additionally, for SBM, nCTRW, and ATTM, EB differs between the original series (colored circles and lines) and their shuffled versions (gray circles and lines). For LW, EB for the original and shuffled series completely coincide. For FBM, EB for the shuffled series for all α coincide with EB for the original series with $\alpha = 0.5$. Hence, gray circles and lines are eclipsed by colored circles and lines for FBM and LW.

unshuffled) and a shuffled version (i.e., a version with the temporal information destroyed) of each process.

1. Accessing fractality using detrended fluctuation analysis

Detrended fluctuation analysis (DFA) computes the Hurst exponent H_{fGn}, quantifying the strength of long-range correlations in series [123,124] using the first-order integration of T-length time series $x(t)$:

$$y(i) = \sum_{k=1}^{i} (x(k) - \overline{x(t)}), \tag{6}$$

where $i = 1, 2, 3, \ldots, T$. DFA computes root mean square (*RMS*; i.e., averaging the residuals) for each linear trend $y_n(t)$ fit to N_n nonoverlapping n-length bins to build a fluctuation

function:

$$f(v,n)=\sqrt{\frac{1}{N_n}\sum_{v=1}^{N_n}\left(\frac{1}{n}\sum_{i=1}^{n}(y((v-1)n+i)-y_v(i))^2\right)}, \tag{7}$$

where $n=\{4,8,12,\dots\}<T/4$. $f(n)$ is a power law,

$$f(n)\sim n^{H_{fGn}}, \tag{8}$$

where H_{fGn} is the scaling exponent estimable using logarithmic transformation:

$$\ln f(n)=H_{fGn}\ln n. \tag{9}$$

Higher H_{fGn} corresponds to stronger long-range correlations.

2. Assessing multifractal spectrum width using the direct-estimation of singularity spectrum

Chhabra and Jensen's [125] direct method estimates multifractal spectrum width $\Delta\alpha$ by sampling a series $x(t)$ at progressively larger scales using the proportion of signal $P_i(n)$ falling within the vth bin of scale n as

$$P_v(n)=\frac{\sum_{k=(v-1)n+1}^{N_n}x(k)}{\sum x(t)}, \tag{10}$$

where $n=\{2,4,8,16,\dots\}<T/8$. As n increases, $P_v(n)$ represents a progressively larger proportion of $x(t)$,

$$P(n)\propto n^{\alpha}, \tag{11}$$

suggesting a growth of the proportion according to one "singularity" strength α [126]. $P(n)$ exhibits multifractal dynamics when it grows heterogeneously across timescales n according to multiple singularity strengths, such that

$$P(n_v)\propto n^{\alpha_v}, \tag{12}$$

whereby each vth bin may show a distinct relationship of $P(n)$ with n. This binning in Chhabra and Jensen's [125] method is a one-dimensional (1D) multifractal elaboration of classical box-counting analyses [126]. The width of this singularity spectrum, $\Delta\alpha=(\alpha_{\max}-\alpha_{\min})$, indicates the heterogeneity of these relationships [127,128].

Chhabra and Jensen's [125] method estimates $P(n)$ for N_n nonoverlapping bins of n sizes and transforms them into a "mass" $\mu(q)$ using a q parameter emphasizing higher or lower $P(n)$ for $q>1$ and $q<1$, respectively, in the form

$$\mu_v(q,n)=\frac{[P_v(n)]^q}{\sum_{j=1}^{N_n}[P_j(n)]^q}. \tag{13}$$

The multifractal analysis is motivated by the cascade dynamics formalism, which involves a variety of fluctuations across different scales that interact with each other. This suggests that there are interactions between events of different sizes, both large and small. One key aspect of the multifractal analysis is using a q parameter, which can be adjusted to accentuate events of different sizes to a greater or lesser extent. By gradually adjusting this parameter, multifractal analysis can create a range of size-accentuated series from a single measurement series. This allows for identifying contributions from fluctuations of different sizes and estimating continuous variation in temporal structure across all sizes. For instance, with $q=1$, all-sized fluctuations are treated similarly, whereas with $q>1$, larger fluctuations are characterized, and with $q<1$, smaller fluctuations are characterized.

Then, $\alpha(q)$ is the singularity for mass μ-weighted $P(n)$ estimated as

$$\begin{aligned}\alpha(q)&=-\lim_{N_n\to\infty}\frac{1}{\ln N_n}\sum_{v=1}^{N_n}\mu_v(q,n)\ln P_v(n)\\&=\lim_{n\to 0}\frac{1}{\ln n}\sum_{v=1}^{N_n}\mu_v(q,n)\ln P_v(n).\end{aligned} \tag{14}$$

Each estimated value of $\alpha(q)$ belongs to the multifractal spectrum only when the Shannon entropy of $\mu(q,n)$ scales with n according to the Hausdorff dimension $f(q)$ [125], where

$$\begin{aligned}f(q)&=-\lim_{N_n\to\infty}\frac{1}{\ln N_n}\sum_{v=1}^{N_n}\mu_v(q,n)\ln\mu_v(q,n)\\&=\lim_{v\to 0}\frac{1}{\ln n}\sum_{v=1}^{N_n}\mu_v(q,n)\ln\mu_v(q,n).\end{aligned} \tag{15}$$

For values of q yielding a strong relationship between Eqs. (14) and (15)—in this study, the correlation coefficient $r>0.995$, the parametric curve $(\alpha(q),f(q))$ or $(\alpha,f(\alpha))$ constitutes the multifractal spectrum and $\Delta\alpha$ (i.e., $\alpha_{\max}-\alpha_{\min}$) constitutes the multifractal spectrum width. r determines only an adequately strong part of the multifractal spectrum is considered. This tradition of using a correlation-coefficient benchmark began with Dixon and Kelty-Stephen [116] trying to operationalize the concerns raised by Zamir [129], and all Kelty-Stephen-co-authored empirical work using Chhabra and Jensen's [125] multifractal analysis since has used this same benchmark. The use of correlation coefficient has regularly provided multifractal spectra whose widths have been significant predictors of various behavioral outcomes [122,130–141]. So, whatever may be arbitrary in this choice of correlation coefficient and whatever may be determined alternatively, equally, more correctly or usefully, the systematic application of this standard across an entire series of experimental datasets has not left the estimated measures of multifractal spectrum width altogether useless.

3. Assessing multifractality due to nonlinearity using surrogate testing

To identify whether a nonzero $\Delta\alpha$ reflects multifractality due to cascade-like interactivity, $\Delta\alpha$ for the original series was compared with $\Delta\alpha$ for 32 iterated amplitude-adjusted Fourier transform (IAAFT) surrogates [142,143]. IAAFT randomizes original values time-symmetrically around the autoregressive structure, generating surrogates that randomize phase ordering of the original series' spectral amplitudes while preserving linear temporal correlations. The one-sample t-statistic (henceforth, t_{MF}) takes the subtractive difference between $\Delta\alpha$ for the original series and the 32 surrogates, dividing by the standard error of the spectrum width for the 32 surrogates. The greater the value of t_{MF}, the greater the

multifractality in the original series due to nonlinear as opposed to linear sources.

D. Estimating ergodicity-breaking parameter EB for FBM, SBM, nCTRW, ATTM, and LW series, and the corresponding TA − MSD, *SD*, *CV*, *RMS*, H_{fGn}, $\Delta\alpha$, and t_{MF} series

Ergodicity can be quantified using a dimensionless statistic of ergodicity breaking EB, also known as the Thirumalai-Mountain metric [95,102] and already mentioned by Rytov *et al.* [99], computed by subtracting the squared total-sample variance from the average squared subsample variance and dividing the resultant by the squared total-sample variance:

$$\mathrm{EB}(x(t)) = \frac{\langle[\overline{\delta^2(x(t))}]^2\rangle - \langle\overline{\delta^2(x(t))}\rangle^2}{\langle\overline{\delta^2(x(t))}\rangle^2}, \tag{16}$$

where $\overline{\delta^2(x(t))} = \int_0^{t-\Delta}[x(t'+\Delta) - x(t')]^2 dt'/(t-\Delta)$ is the time-average mean-squared displacement of the stochastic series $x(t)$ for lag time Δ. This relationship is effectively the variance of sample variance divided by the total-sample squared variance. Rapid decay of EB to 0 for progressively larger samples (i.e., EB $\to 0$ as $t \to \infty$ implies ergodicity). Thus, for Brownian motion $\mathrm{EB}(x(t)) = \frac{4}{3}(\frac{\Delta}{t})$ [144,145]. Slower decay indicates less ergodic systems in which trajectories are less reproducible, and no decay or convergence to a finite asymptotic value indicates strong ergodicity breaking [104]. EB$(x(t))$ thus allows testing whether a given time series fulfills ergodic assumptions or breaks ergodicity and the extent to which it breaks ergodicity.

For instance, Deng and Barkai [104] have shown that for FBM,

$$\mathrm{EB}(x(t)) = \begin{cases} k(H_{fGn})\frac{\Delta}{t} & \text{if } 0 < H_{fGn} < \frac{3}{4} \\ k(H_{fGn})\frac{\Delta}{t}\ln t & \text{if } H_{fGn} = \frac{3}{4} \\ k(H_{fGn})\left(\frac{\Delta}{t}\right)^{4-4H_{fGn}} & \text{if } \frac{3}{4} < H_{fGn} < 1. \end{cases} \tag{17}$$

Likewise, Thiel and Sokolov [146] have shown that, for SBM,

$$\mathrm{EB}(x(t)) = \begin{cases} 4Z_\alpha\left(\frac{\Delta}{t}\right)^{2\alpha} & \text{if } \alpha \leqslant \frac{1}{2} \\ \frac{4\alpha^2}{3(2\alpha-1)}\frac{\Delta}{t} & \text{if } \alpha > \frac{1}{2}, \end{cases} \tag{18}$$

where $Z_\alpha = \int_0^1 dy \int_0^\infty dx[(x+1)^\alpha - (x+y)^\alpha]^2$. For any positive value of the anomalous exponent α, EB for SBM vanishes and shows a crossover between two types of t dependence at $\alpha = 1/2$ [146]. Compare also [92]. Despite the vanishing EB, SBM is weakly nonergodic, i.e., ensemble and time averages are disparate.

We computed EB for the absolute values obtained for the original and a shuffled version of each process (range $=T/50$; lag $\Delta = 10$ samples) as Eq. (16).

We computed EB for TA-MSD for the original and a shuffled version of each process (range $= T/50$; lag $\Delta = 10$ samples) as

$$\mathrm{EB}(\text{TA-MSD}(t)) = \frac{\langle[\overline{\delta^2(\text{TA-MSD}(t))}]^2\rangle - \langle\overline{\delta^2(\text{TA-MSD}(t))}\rangle^2}{\langle\overline{\delta^2(\text{TA-MSD}(t))}\rangle^2}. \tag{19}$$

We computed EB for *SD*, *CV*, *RMS*, H_{fGn}, $\Delta\alpha$, and t_{MF} series computed over the 100 nonoverlapping segments for the original and a shuffled version of each process (range $=s/2$; lag $\Delta = 1$ segment, where s denotes the 100 nonoverlapping 500-sample segments over which each of these descriptors were computed, such that $s = \{s_1, s_2, \ldots, s_{100}\}$) as

$$\mathrm{EB}(SD(s)) = \frac{\langle[\overline{\delta^2(SD(s))}]^2\rangle - \langle\overline{\delta^2(SD(s))}\rangle^2}{\langle\overline{\delta^2(SD(s))}\rangle^2}, \tag{20}$$

$$\mathrm{EB}(CV(s)) = \frac{\langle[\overline{\delta^2(CV(s))}]^2\rangle - \langle\overline{\delta^2(CV(s))}\rangle^2}{\langle\overline{\delta^2(CV(s))}\rangle^2}, \tag{21}$$

$$\mathrm{EB}(RMS(s)) = \frac{\langle[\overline{\delta^2(RMS(s))}]^2\rangle - \langle\overline{\delta^2(RMS(s))}\rangle^2}{\langle\overline{\delta^2(RMS(s))}\rangle^2}, \tag{22}$$

$$\mathrm{EB}(H_{fGn}(s)) = \frac{\langle[\overline{\delta^2(H_{fGn}(s))}]^2\rangle - \langle\overline{\delta^2(H_{fGn}(s))}\rangle^2}{\langle\overline{\delta^2(H_{fGn}(s))}\rangle^2}, \tag{23}$$

$$\mathrm{EB}(\Delta\alpha(s)) = \frac{\langle[\overline{\delta^2(\Delta\alpha(s))}]^2\rangle - \langle\overline{\delta^2(\Delta\alpha(s))}\rangle^2}{\langle\overline{\delta^2(\Delta\alpha(s))}\rangle^2}, \tag{24}$$

$$\mathrm{EB}(t_{MF}(s)) = \frac{\langle[\overline{\delta^2(t_{MF}(s))}]^2\rangle - \langle\overline{\delta^2(t_{MF}(s))}\rangle^2}{\langle\overline{\delta^2(t_{MF}(s))}\rangle^2}, \tag{25}$$

respectively.

III. RESULTS

A. Ergodicity breaking depends on the type of the diffusion process and the anomalous exponent α

We observe noteworthy ergodicity-related differences across the five types of anomalous diffusion processes and different values of the anomalous exponent α. FBM for smaller values of α (i.e., $\alpha \to 0.1$) and SBM for larger values of α (i.e., $\alpha \to 1$) return and converge towards the mean, suggestive of ergodicity [Fig. 2(a)]. EB$(x(t))$ confirmed this observation. For FBM, EB $\to 0$ as $\alpha \to 0.1$, and for SBM, EB $\to 0$ as $\alpha \to 1$ [Fig. 2(b)]. FBM appears to break ergodicity for larger values of α, indicated by little to no decay in EB with t. SBM appears to break ergodicity for smaller values of α, which, despite decay in EB with t, do not even reach 1. The observation further confirms ergodicity in FBM and SBM that the EB$(x(t))$ curves almost entirely coincide for the original and shuffled trajectories as $\alpha \to 0.1$ for FBM and $\alpha \to 1$ for SBM, indicating that these processes behaved as awGn. In contrast, the EB$(x(t))$ curves for the original and shuffled versions coincide to progressively lesser extent as $\alpha \to 1$ for FBM and $\alpha \to 0.1$ for SBM. Overall, not only EB for the five processes does not converge to an acceptably small value within our observation time, the FBM, SBM, nCTRW, ATTM, and LW trajectories show highly variable rates of decays in EB: $\mathrm{EB}(x(t)) = -1.01\frac{\Delta}{t}$ to $-0.18\frac{\Delta}{t}$, $-1.05\frac{\Delta}{t}$ to $-0.42\frac{\Delta}{t}$, $-1.11\frac{\Delta}{t}$ to $-0.25\frac{\Delta}{t}$, $-1.87\frac{\Delta}{t}$ to $-0.45\frac{\Delta}{t}$, and $-1.02\frac{\Delta}{t}$ to $-0.99\frac{\Delta}{t}$, respectively, where Δ in $\frac{\Delta}{t} = 10$, not atypical values for many empirical data.

Unlike FBM and SBM, nCTRW, ATTW, and LW diverge and never return toward the mean, suggesting ergodicity breaking in these processes [Fig. 2(a)]. EB quickly decays

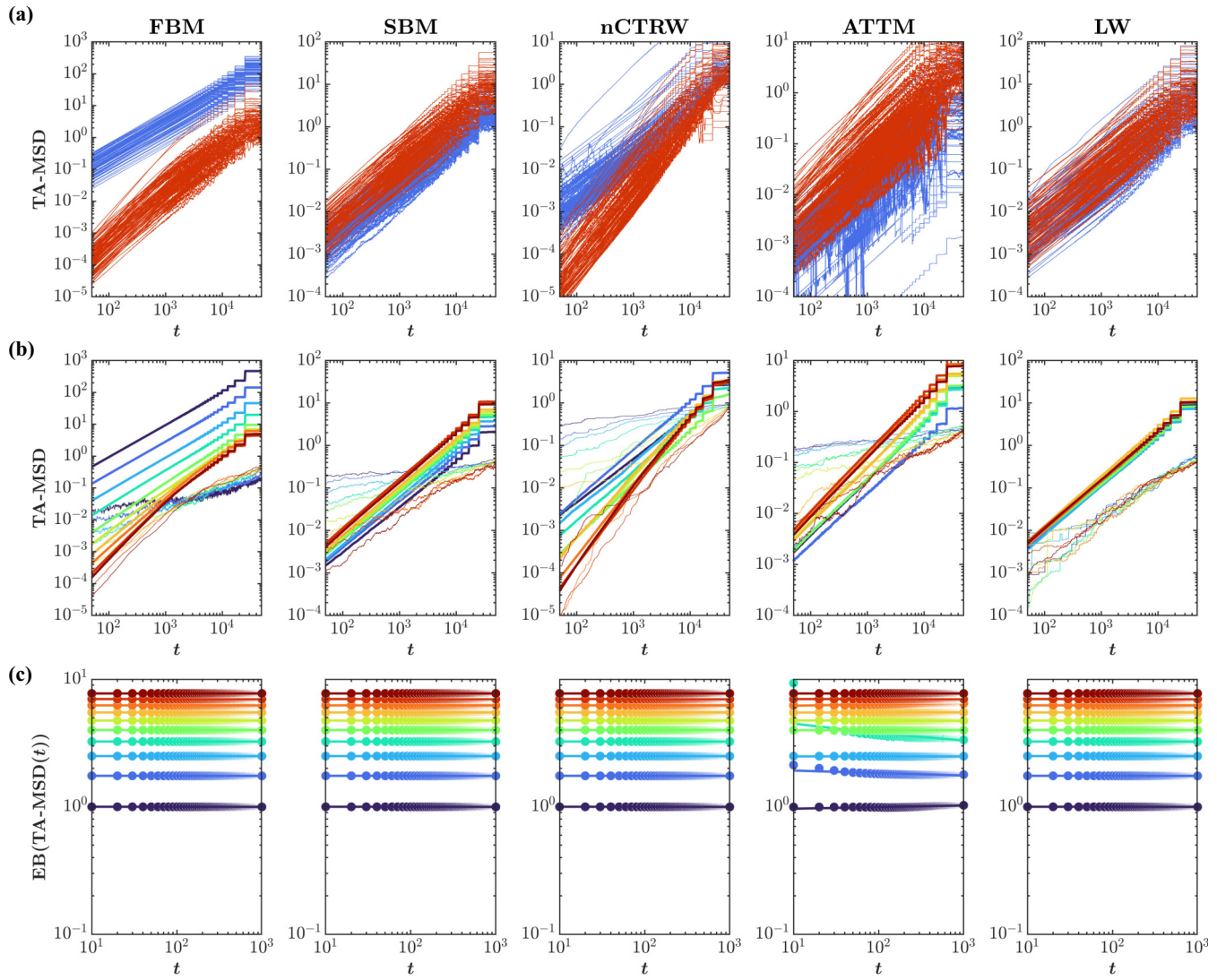

FIG. 3. Ergodicity breaking in TA-MSD. (a) TA-MSD for 100 simulated trajectories of the five anomalous diffusion processes—FBM, SBM, nCTRW, ATTM, and LW, for two values of the anomalous exponent α blue: $\alpha = 0.2$ for nCTRW, ATTM, FBM, and SBM, and $\alpha = 1.2$ for LW; red: $\alpha = 0.9$ for nCTRW, ATTM, FBM, and SBM, and $\alpha = 1.9$ for LW. (b) EA-MSD (colored thick lines) and TA-MSD (colored thin lines) for the five anomalous diffusion processes—FBM, SBM, nCTRW, ATTM, and LW. The anomalous exponent α ranges from 0.1 to 1 for FBM, SBM, nCTRW, and ATTM and from 1.1 to 2 for LW, with an increment of 0.1 from dark blue to dark red. (c) EBTA-MSD(s) for the five processes and different values of α ($N = 100$; lag is $\Delta = 10$ samples). The EB(TA-MSD(t)) curves all coincide at 10^0 but have been shifted vertically for convenience of presentation, and hence, the vertical axis is given in arbitrary units.

with t but does not even reach 1 for nCTRW and ATTW for smaller values of α (i.e., $\alpha \to 0.1$) and for LW for all values of α, suggestive of weak ergodicity breaking [Fig. 2(b)]. EB showed little to no decay with t for nCTRW and ATTW for larger values of α (i.e., $\alpha \to 1$), suggestive of stronger breaking of ergodicity. This ergodicity breaking of nCTRW and ATTW is further confirmed by the finding that the EB($x(t)$) for the original and shuffled nCTRW and ATTW coincide to progressively lesser extent as $\alpha \to 1$. LW showed the weakest ergodicity breaking, wherein EB quickly decays with t for all values of α but does not reach 1. Hence, FBM and SBM break ergodicity for larger and smaller values of the anomalous exponent α, nCTRW, ATTM, and SBM break ergodicity to differential extents.

B. TA-MSD reflects ergodicity-related differences among different anomalous diffusion processes

Figures 3(a) and 3(b) show that TA-MSD grows with lag time Δ for all five types of anomalous diffusion processes—FBM, SBM, nCTRW, ATTM, and LW—in the entire range of Δ. (The individual amplitudes scatter owing to the stochasticity in generating these trajectories. Such scatter characteristics of anomalous diffusion processes can be used to reliably distinguish between FBM from nCTRW processes; see, for instance, Refs. [111,147].) Furthermore, TA-MSD growth shows differential dependence on the anomalous exponent α across the five processes. For example, this dependence was strongest for FBM and lowest for LW, suggesting that the growth rates of TA-MSD might not provide sufficient

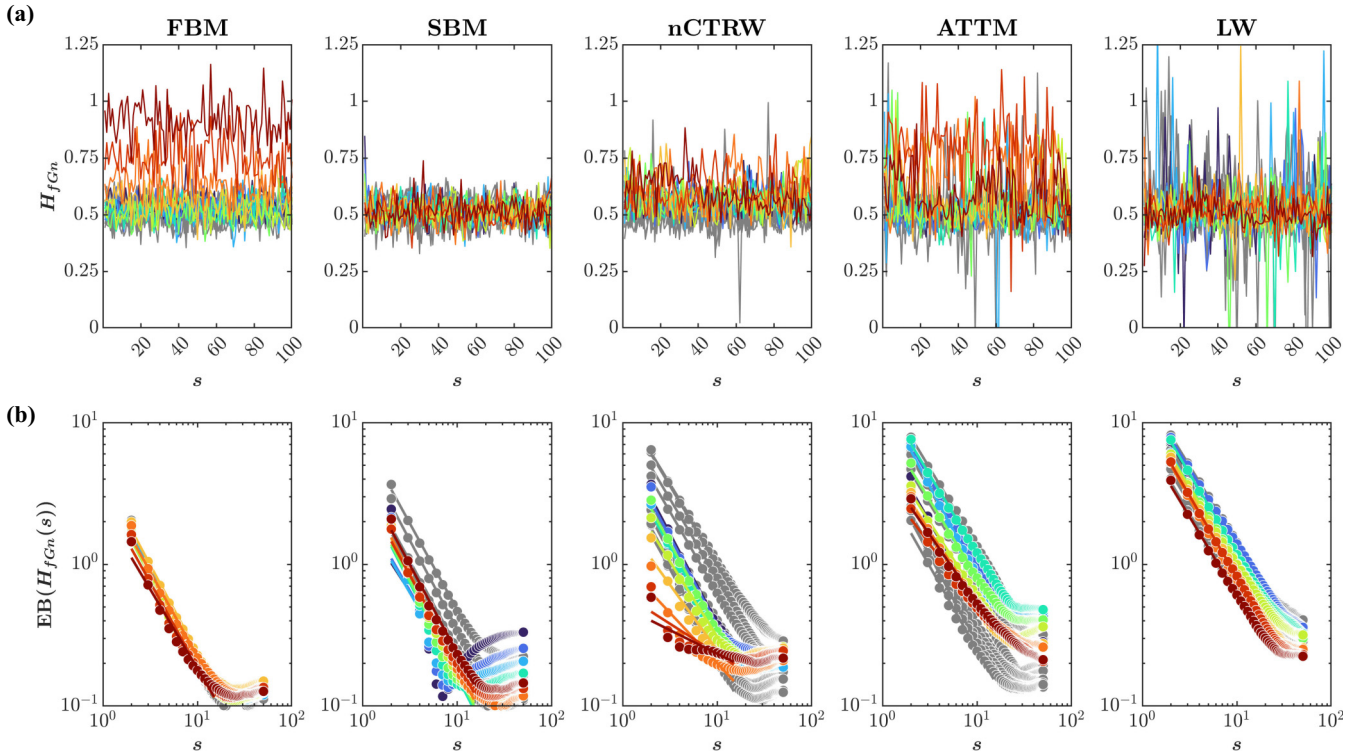

FIG. 4. Ergodicity breaking in the strength of temporal correlations, H_{fGn}. (a) Representative H_{fGn} series (H_{fGn} calculated across the 100 nonoverlapping 500-sample segments) for the five anomalous diffusion processes—FBM, SBM, nCTRW, ATTM, and LW. The anomalous exponent α ranges from 0.1 to 1 for FBM, SBM, nCTRW, and ATTM and from 1.1 to 2 for LW, with an increment of 0.1 from dark blue to dark red. Gray trajectories indicate H_{fGn} series for the corresponding shuffled versions. (b) EB($H_{fGn}(s)$) for the five processes and different values of α ($N = 100$; lag is $\Delta = 1$ segment). Gray curves indicate mean EB($H_{fGn}(s)$) for the corresponding shuffled versions.

resolution to distinguish multiple trajectories of the same process with different anomalous exponents. EB for TA-MSD remains constant across t [Fig. 3(c)]; indeed, TA-MSD for FBM, SBM, nCTRW, ATTM, and LW show no decay whatsoever in EB: EB(TA-MSD(t)) = 0 for all values of the anomalous exponent α. Hence, TA-MSD mask any ergodicity-related differences among the five processes and processes with different anomalous exponents and cannot be used as a stable causal predictor in the linear modeling of cause-effect relationships in this type of analysis.

C. MSD-related linear descriptors such as *SD*, *CV*, and *RMS* reflect ergodicity-related differences among different anomalous diffusion processes

SD for FBM for all values of the anomalous exponent α and SBM for $\alpha = 1$—the case in which SBM is reduced to awGn—return and converges towards the mean, suggestive of ergodicity. In contrast, *SD* for SBM, nCTRW, ATTW, and LW diverge and never return towards the mean, suggesting ergodicity breaking in the *SD* series for these processes. EB(*SD*(s)) confirmed these trends (see Appendix B). Except for some minor differences, the ergodicity-breaking behavior of *CV* resembles that of *SD*, and the *RMS* series behaved exactly as the *SD* series for all five processes (see Appendix B).

D. Multifractal descriptors provide an ergodic characterization of nonergodic anomalous diffusion processes

The H_{fGn} series—quantifying the strength of temporal correlations in each of the 100 nonoverlapping 500-sample segments of the synthetic trajectories—shows signs of restoring ergodicity to the description of some of these processes. The H_{fGn} series for FBM behaved ergodically (i.e., EB $\to 0$ as $s \to \infty$) independent of the anomalous exponent α, and so do H_{fGn} series for LW (Fig. 4). However, the H_{fGn} series for LW show a marginal dependence on α, as the EB taper off at higher values of s. The observation further strengthens this result that EB($H_{fGn}(s)$) curves entirely coincide with the original and shuffled trajectories. The H_{fGn} series for SBM show strong ergodicity breaking with EB initially having a converging-to-zero trend but then taking an upward turn and increasing with s for the rest of the range. The only exception to this trend is the H_{fGn} series for the SBM trajectories for $\alpha = 1$—in which SBM is reduced to awGn. The H_{fGn} series for CTRW and ATTM also behaved ergodically with a few exceptions: the H_{fGn} series for CTRW break ergodicity at larger values of α and the H_{fGn} series for the original and shuffled ATTM trajectories diverge with increasing α. On average, the H_{fGn} series for FBM, SBM, nCTRW, ATTM, and LW show the initial rates of decay in EB: EB($H_{fGn}(s)$) $= -1.23\frac{\Delta}{s}$, $-1.23\frac{\Delta}{s}$, $-0.97\frac{\Delta}{s}$, $-1.08\frac{\Delta}{s}$, and $-1.12\frac{\Delta}{s}$, respectively, where $\Delta = 1$ (Table I). In other words, the H_{fGn} series for the five processes show very similar rates of decay in EB.

TABLE I. The slopes of EB($\Delta\alpha(s)$) for the five anomalous diffusion processes and different values of α in terms of $\frac{\Delta}{s}$.

α[a]	FBM	SBM	cCTRW	ATTM	LW
0.1 (1.1)	−1.26	−1.03	−1.27	−1.16	−1.11
0.2 (1.2)	−1.23	−1.16	−1.25	−1.21	−1.07
0.3 (1.3)	−1.25	−1.15	−1.27	−1.25	−1.13
0.4 (1.4)	−1.26	−1.32	−1.21	−1.10	−1.14
0.5 (1.5)	−1.28	−1.30	−1.21	−1.08	−1.08
0.6 (1.6)	−1.27	−1.33	−1.06	−1.04	−1.08
0.7 (1.7)	−1.26	−1.26	−0.92	−1.06	−1.16
0.8 (1.8)	−1.20	−1.31	−0.71	−0.98	−1.21
0.9 (1.9)	−1.20	−1.22	−0.43	−0.89	−1.15
1 (2)	−1.12	−1.24	−0.33	−0.96	−1.10

[a]The anomalous exponent α ranges from 0.1 to 1 for FBM, SBM, nCTRW, and ATTM and from 1.1 to 2 for LW (in parentheses).

The $\Delta\alpha$ series—quantifying the width of the multifractal spectrum in each of the 100 nonoverlapping 500-sample segments of the synthetic trajectories—also show signs of restoring ergodicity to all five processes, albeit with some exceptions pertaining to specific values of the anomalous exponent. The $\Delta\alpha$ series for FBM behave ergodically (i.e., EB $\to 0$ as $s \to \infty$) independent of α, and so do the $\Delta\alpha$ series for LW (Fig. 5). However, the $\Delta\alpha$ series for LW show marginal dependence on α, as EB taper off at higher values of s. The $\Delta\alpha$ series for SBM show strong ergodicity breaking with EB initially having a converging-to-zero trend but then taking an upward turn and increasing with s for the rest of the range. The only exception to this trend is the $\Delta\alpha$ series for the SBM trajectories for $\alpha = 1$—in which SBM is reduced to awGn. The $\Delta\alpha$ series for CTRW and ATTM also behave ergodically with a few exceptions: the $\Delta\alpha$ series for CTRW break ergodicity at larger values of α, and the $\Delta\alpha$ series for the original and shuffled ATTM trajectories diverge with increasing α. On average, the $\Delta\alpha$ series for FBM, SBM, nCTRW, ATTM, and LW show the average initial rates of decay in EB: EB($\Delta\alpha(s)$) $= -1.23\frac{\Delta}{s}$, $-1.22\frac{\Delta}{s}$, $-0.93\frac{\Delta}{s}$, $-1.12\frac{\Delta}{s}$, and $-1.16\frac{\Delta}{s}$, respectively, where $\Delta = 1$ (Table II).

The t_{MF} series—quantifying multifractality due to nonlinearity in each of the 100 nonoverlapping 500-sample segments of the synthetic trajectories—for all five processes—FBM, SBM, nCTRW, ATTM, and LW—show a rapid decay of EB with a progressively larger sample of segments, i.e., EB $\to 0$ as $s \to 0$ for $t \to \infty$ (Fig. 6). On average, the t_{MF} series for FBM, SBM, nCTRW, ATTM, and LW show the average initial rates of decay in EB: EB($t_{MF}(s)$) $= -1.20\frac{\Delta}{s}$, $-1.24\frac{\Delta}{s}$, $-1.20\frac{\Delta}{s}$, $-1.17\frac{\Delta}{s}$, and $-1.20\frac{\Delta}{s}$, respectively, where $\Delta = 1$ (Table III). In other words, the t_{MF} series for the five processes do not vary in the initial decay rates in EB. Moreover, EB($t_{MF}(s)$) shows a marginal dependence on the anomalous exponent α at higher values of s, except for ATTM for which EB($t_{MF}(s)$) shows marginally higher dependence on α. Notably, the EB($t_{MF}(s)$) curves entirely coincide for the original

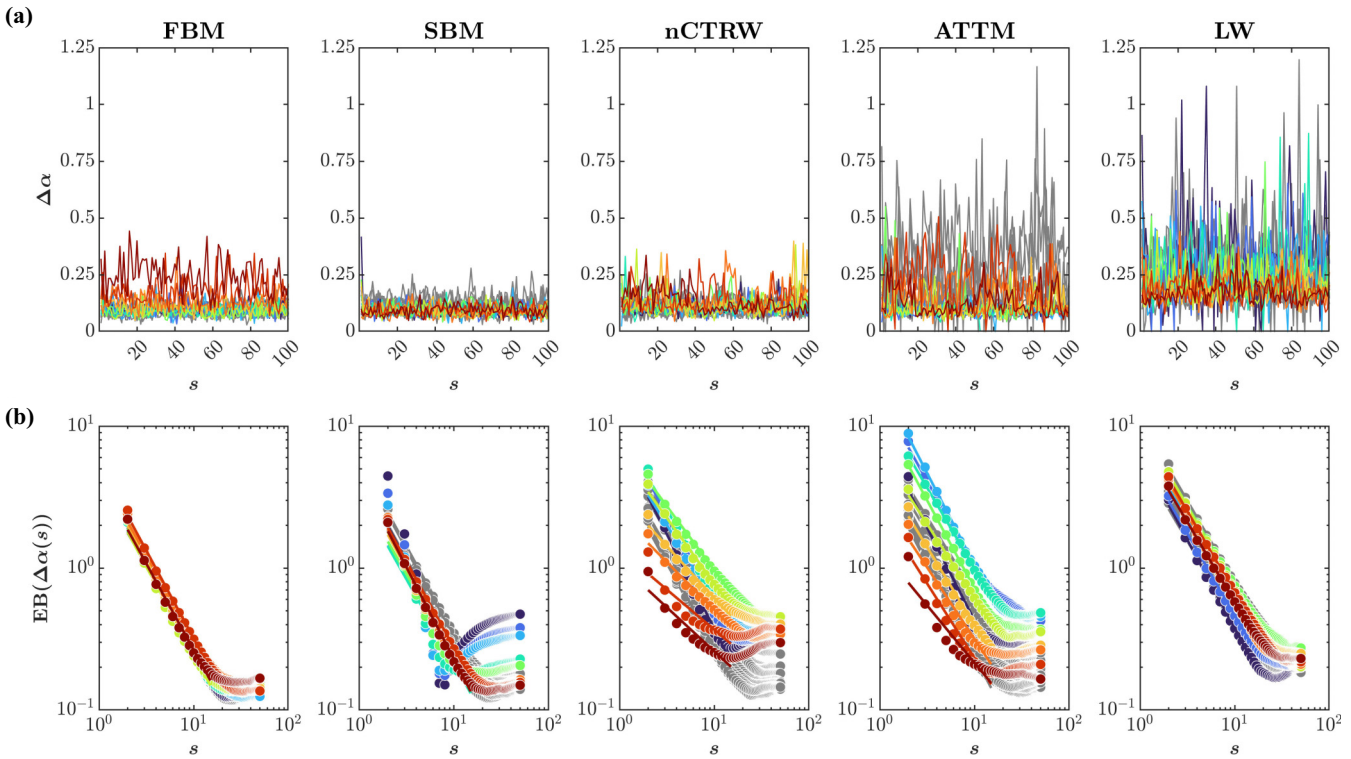

FIG. 5. Ergodicity breaking in multifractal spectrum width, $\Delta\alpha$. (a) Representative $\Delta\alpha$ series ($\Delta\alpha$ calculated across the 100 nonoverlapping 500-sample segments) for the five anomalous diffusion processes—FBM, SBM, nCTRW, ATTM, and LW. The anomalous exponent α ranges from 0.1 to 1 for FBM, SBM, nCTRW, and ATTM and from 1.1 to 2 for LW, with an increment of 0.1 from dark blue to dark red. Gray trajectories indicate $\Delta\alpha$ series for the corresponding shuffled versions. (b) Mean EB($\Delta\alpha(s)$) for the five processes and different values of α ($N = 100$; lag is $\Delta = 1$ segment). Gray curves indicate mean EB($\Delta\alpha(s)$) for the corresponding shuffled versions.

TABLE II. The slopes of EB($H_{fGn}(s)$) for the five anomalous diffusion processes and different values of α in terms of $\frac{\Delta}{s}$.

α[a]	FBM	SBM	cCTRW	ATTM	LW
0.1 (1.1)	−1.28	−1.24	−1.33	−1.31	−1.24
0.2 (1.2)	−1.20	−1.22	−1.32	−1.19	−1.15
0.3 (1.3)	−1.29	−1.12	−1.07	−1.29	−1.16
0.4 (1.4)	−1.25	−1.18	−1.13	−1.14	−1.17
0.5 (1.5)	−1.20	−1.17	−0.90	−1.24	−1.13
0.6 (1.6)	−1.23	−1.27	−0.92	−0.03	−1.18
0.7 (1.7)	−1.18	−1.22	−0.73	−0.09	−1.13
0.8 (1.8)	−1.19	−1.26	−0.67	−0.01	−1.20
0.9 (1.9)	−1.24	−1.21	−0.56	−0.05	−1.15
1 (2)	−1.22	−1.29	−0.62	−0.81	−1.12

[a]The anomalous exponent α ranges from 0.1 to 1 for FBM, SBM, nCTRW, and ATTM and from 1.1 to 2 for LW (in parentheses).

TABLE III. The slopes of EB($t_{MF}(s)$) for the five anomalous diffusion processes and different values of α in terms of $\frac{\Delta}{s}$.

α[a]	FBM	SBM	cCTRW	ATTM	LW
0.1 (1.1)	−1.26	−1.24	−1.22	−1.24	−1.39
0.2 (1.2)	−1.19	−1.29	−1.26	−1.25	−1.16
0.3 (1.3)	−1.26	−1.28	−1.21	−1.30	−1.18
0.4 (1.4)	−1.21	−1.23	−1.28	−1.26	−1.17
0.5 (1.5)	−1.18	−1.25	−1.24	−1.17	−1.19
0.6 (1.6)	−1.23	−1.22	−1.28	−1.08	−1.20
0.7 (1.7)	−1.19	−1.22	−1.23	−1.21	−1.14
0.8 (1.8)	−1.18	−1.23	−1.13	−1.05	−1.20
0.9 (1.9)	−1.20	−1.18	−1.08	−1.08	−1.16
1 (2)	−1.16	−1.28	−1.10	−1.06	−1.22

[a]The anomalous exponent α ranges from 0.1 to 1 for FBM, SBM, nCTRW, and ATTM and from 1.1 to 2 for LW (in parentheses).

and shuffled trajectories, demonstrating that the ergodic behavior of the t_{MF} series for the original series did not differ from the shuffled versions that lack any temporal correlations found in the original trajectories. Hence, the t_{MF} series fully restore broken ergodicity to a description of all five diffusion processes and all values of α. This result strongly resonates with previous findings on $1/f$ noise, $1/f$ noise with different levels of non-Gaussianity, and binomial multiplicative cascades [105,106,108].

E. Multifractal spectrum distinguish different anomalous diffusion processes

Figure 7(a) shows the multifractal spectrum for the five processes—FBM, SBM, nCTRW, ATTM, and LW and different values of the anomalous exponent α. FBM shows highly symmetric spectra with initially fleeting and increasing differences between the original spectrum and the corresponding IAAFT surrogates for larger α. This trend is confirmed by an initially fleeting and then increasing percentage of FBM trajectories with the wider-than-surrogate spectrum and an

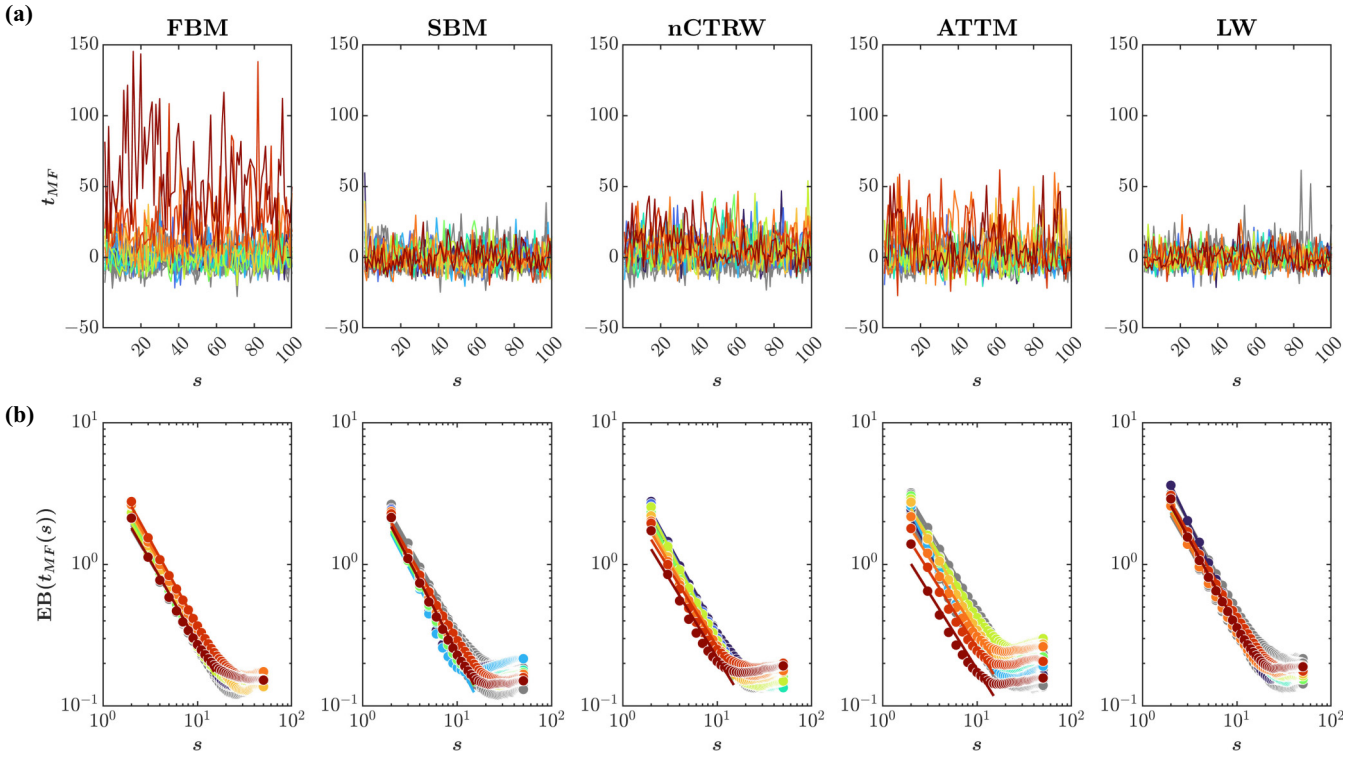

FIG. 6. Ergodicity breaking in multifractal nonlinearity, t_{MF}. (a) Representative t_{MF} series (t_{MF} calculated across the 100 nonoverlapping 500-sample segments) for the five anomalous diffusion processes—FBM, SBM, nCTRW, ATTM, and LW. The anomalous exponent α ranges from 0.1 to 1 for FBM, SBM, nCTRW, and ATTM and from 1.1 to 2 for LW, with an increment of 0.1 from dark blue to dark red. Gray trajectories indicate t_{MF} series for the corresponding shuffled versions. (b) EB($t_{MF}(s)$) for the five processes and different values of α ($N = 100$; lag is $\Delta = 1$ segment). Gray curves indicate mean EB($t_{MF}(s)$) for the corresponding shuffled versions.

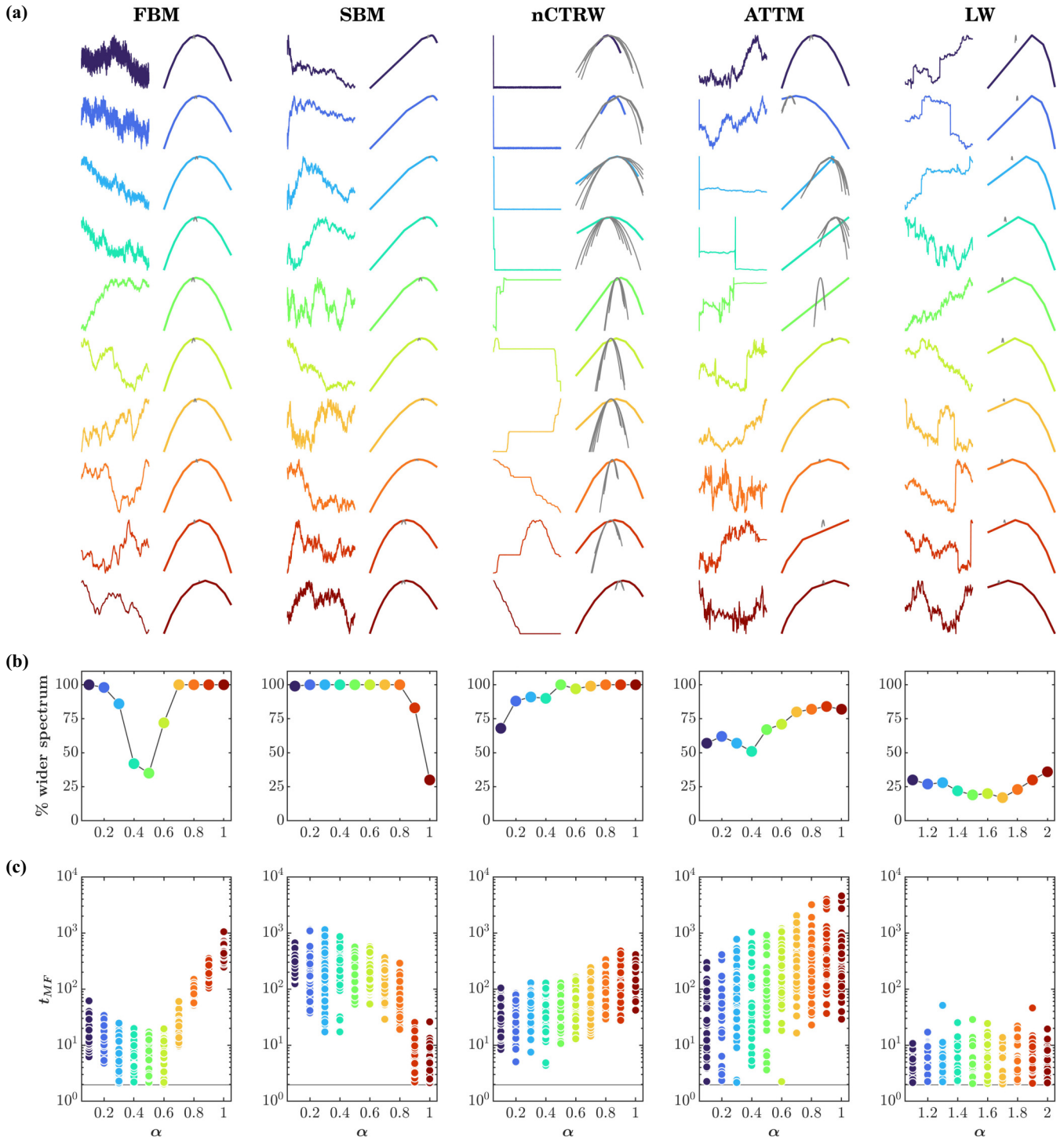

FIG. 7. Multifractal formalism appears to be a nonlinear analytical method that unifies several disparate nonergodic anomalous diffusion processes into a common framework of multiplicative cascades. (a) Multifractal spectrum for the five types of anomalous diffusion processes—FBM, SBM, nCTRW, ATTM, and LW. The anomalous exponent α ranges from 0.1 to 1 for FBM, SBM, nCTRW, and ATTM and from 1.1 to 2 for LW, with an increment of 0.1 from dark blue to dark red. The thick colored curve in each plot indicates the multifractal spectrum for the original series, and the thin gray curves in each plot indicate the multifractal spectrum for a sample of five corresponding IAAFT surrogates. The axes have been stretched to match the minimum and maximum values of $(\alpha(q), f(q))$. In some cases, the gray lines representing the IAAFT surrogates may be hardly discernible because the spectrum associated with these surrogates is significantly smaller than the spectrum of the original series. (b) The percentage of simulated trajectories with the wider-than-surrogates spectrum, i.e., $t_{MF} > 1.96$. (c) Multifractal nonlinearity t_{MF} for processes with the wider-than-surrogates spectrum.

initially fleeting and then increasing t_{MF} values with an increase in α [Figs. 7(b) and 7(c)].

SBM shows highly asymmetric multifractal spectra, with the completely missing right half of the spectrum and with the spectra becoming more asymmetric with an increase in α and resembling the spectra for FBM at $\alpha = 1$—the case in which SBM is reduced to awGn [Fig. 7(a)]. This asymmetry reflects the putative effects of large q moments, which exacerbate the effects of smaller fluctuations in estimating the multifractal spectrum. The difference between the original spectrum and those of the corresponding IAAFT surrogates is more prominent for smaller values of α, a trend which was confirmed by the reduction in t_{MF} values with an increase in α [Fig. 7(c)].

nCTRW shows asymmetric multifractal spectra throughout but a more leftward skewed spectrum for $\alpha \to 1$ [Fig. 7(a)]. Again, this asymmetry reflects the putative effects of small q moments, which exacerbate the effects of larger fluctuations in estimating the multifractal spectrum. However, despite these fluctuations in the asymmetry of the multifractal spectrum, the difference between the original spectrum and those of the corresponding IAAFT surrogates increase sharply with α, a trend confirmed by the increase in the percentage of nCTRW trajectories with the wider-than-surrogate spectrum and an increase in t_{MF} values with an increase in α [Figs. 7(b) and 7(c)].

ATTM shows highly asymmetric and distorted multifractal spectra, but the skew direction does not depend on α in a principled way [Fig. 7(a)]. Nonetheless, the difference between the original spectrum and those of the corresponding IAAFT surrogates increased sharply with α. While the percentage of ATTM trajectories with the wider-than-surrogate spectrum increase with α [Fig. 7(b)], t_{MF} values show only marginal increase with α [Fig. 7(c)].

LW shows highly asymmetric multifractal spectra, almost with the missing left half of the spectrum when $\alpha \to 1$ [Fig. 7(a)]. This asymmetry reflects the putative effects of small q moments, which exacerbate the effects of larger fluctuations in estimating the multifractal spectrum. The spectra of the original trajectories and the corresponding IAAFT surrogates also do not differ in a principled manner. This ambiguity is evident in the low percentage of LW trajectories with wider-than-surrogate spectrum [<50 out of 100; Fig. 7(b)] and comparable t_{MF} values across all α [Fig. 7(c)].

In short, the five anomalous diffusion processes all show multifractal evidence of nonlinearities, albeit minor differences in the percentage of trajectories showing multifractal evidence and the strength of evidence. Notably, the shape of the multifractal spectrum reflected the respective generative mechanism—e.g., symmetric spectra for FBM, left-slewed spectra for SBM, and right-skewed spectra for LW, reflecting that smaller and larger fluctuations, respectively, characterize these two processes. While more detailed interpretations warrant further investigations, it is evident that multifractal analysis can diagnose certain differences among these anomalous diffusion processes.

IV. DISCUSSION

This work explores preliminary steps towards a unified framework grounded in the multifractal formalism [121,142,148] for restoring ergodicity to a description of anomalous diffusion processes [149–151]. We used synthetic data representing various anomalous diffusion processes for a wide range of anomalous exponent α, both ergodic and nonergodic, approximated by five disparate mathematical models: FBM, ergodic; SBM, weakly nonergodic; CTRW, weakly nonergodic; ATTM, weakly nonergodic; and LW, ultraweakly nonergodic. We show that TA-MSD and MSD-related linear descriptors such as SD, CV, and RMS break ergodicity. In contrast, time series of descriptors addressing sequential structure and its potential nonlinearity: multifractality, and, to some extent, fractality, change in a time-independent way and are ergodic descriptors insensitive to the weak ergodicity breaking of the process. Thus, these descriptors return the same information for any diffusion process and the anomalous exponent α. Further analysis revealed that these findings directly followed the multiplicative cascades underlying these diffusion processes, as the shape and symmetry of the multifractal spectrum—and those of the corresponding surrogate series—differentiated these processes. Thus, the statistical descriptors analyzed here provide very different, complementary information to other statistical descriptors. Two particular points bear emphasis here. First, because multifractal descriptors of anomalous diffusion remain ergodic, they can be submitted to linear causal modeling. Second, this capacity to describe nonergodic anomalous diffusion processes in ergodic terms offers the possibility that multifractal modeling could unify these processes into a common framework.

Multifractal formalisms can serve as the desired analytical framework for linear causal modeling of anomalous diffusion processes. Whereas TA-MSD and TA-MSD-related linear descriptors like SD, CV, and RMS that are typically submitted to linear causal models [152–154] break ergodicity [105,107,108]. In contrast, multifractal descriptors remain ergodic and hence, offer a reliable and stable set of causal predictors [116,118,122,131,132,134,137,155–159]. Although MSD remains prevalent in measuring active matter, our present results resonate with a growing interest in multifractal modeling in many of these active-matter fields, e.g., biomolecules moving within cells [160–163], animals foraging in the wild [164–167], and the emergence of collective dynamics such as swarming and milling [132,168,169], have begun to embrace multifractal formalisms. We hope that the current findings might emphasize the importance of these approaches.

The ergodicity of multifractal descriptors allows the possibility that cascade dynamics constitute a statistically testable causal framework that may explain these disparate anomalous-diffusion regimes. The findings underscore that multifractal structure is not merely an abstract side effect, nor is it a nuisance to collapse into the noise terms to avoid cluttering the lower-dimensional aspects of our generative models [170,171]. The accumulating evidence of multifractal structure and its relevance for describing and predicting structural change has implicated a causal role in cascading dynamics [89,118,172]. Indeed, the high-dimensional aspect of cascade dynamics sometimes raises new and unfamiliar questions about the relationship between causality and low-dimensional determinism. Indeed, we may feel most confident explaining when we have reduced our model systems to a minimal set of control parameters. That confidence

may lead us to take for granted that the low-dimensional constraint needed for deterministic modeling is required to model and explain causal relationships. Our commitment to low-dimensional causation is so strong that scholars will even reason that low-dimensionality and so determinism is a matter of observer's knowledge: e.g., the suggestion that, if only we knew how the system works, then we might no doubt see that causation is low-dimensional after all [173]. However, the mutually fostering growth of multifractal estimation and cascade-dynamical modeling has strengthened the possibility that causation may not need low dimensionality. Philosophical, logical, and empirical approaches have all begun to point to growing comfort and fluency with the concepts of stochastic causation [172,174–177], and even stochastic-deterministic blends that reflect the cascade-like dynamics across multiple scales [178].

The observed variety of multifractal spectrum across the five simulated anomalous diffusion processes suggests that multifractal formalisms could also aid in time-series characterization and clustering. The generation rate of time series is exponentially increasing in all areas of physical and life sciences, and the production of ad hoc analytical tools accompanies this growth [179–181]. Many of these attempts use Bayesian [71–75] and ML approaches [50,76–80], and even unsupervised [81–86] to detect specific anomalous diffusion processes and the underlying mathematical model, especially deviation from pure Brownian behavior in terms of the anomalous exponent. However, these attempts still lack the accuracy, sensitivity, and specificity necessary, say, for understanding how diffusion properties change over time due to environmental heterogeneity (e.g., patches with different viscosity on a cellular membrane), time-varying properties of the observable (e.g., different activation states of a molecular motor). This limitation may reflect that these attempts typically rely on manual or automatic extraction of features that may not have to do with plausible generating mechanisms [87,88]. Including multifractal descriptors with MSD-related linear descriptors might improve the ML-powered characterization and clustering of anomalous diffusion processes.

Interdependent fluctuations can cause interactions across various spatiotemporal scales, altering the context for subsequent fluctuations. Cascade instabilities, e.g., can produce turbulent structures, complex flows in which once-parallel currents collapse or explode into a dizzying, possibly limitless variety of vortices and eddies, with intermittent swelling and ebbing throughout space and time [89,93,182]. Indeed, anomalous diffusion and Lévy walks distinguish active from inertial turbulence [19]. Our results indicate that the various diffusion coefficients are interconnected with the specific geometries of fluctuations constituting the measured series. The connection between multifractality and various models of anomalous diffusion is also being noticed both theoretically [54,183–186] and empirically [166,167,172,187–190]. Multifractal formalisms and anomalous-diffusion processes thus appear to be entwined in a vibrant, expanding, far-reaching, and synergistic relationship originating from the out-of-equilibrium character, lack of detailed balance, and of time-reversal symmetry, multiscale nature, nonlinearity and multibody interactions that typify living and evolving systems [191]. Future investigations could further explore the relationship between the various features of the multifractal spectrum and anomalous diffusion.

ACKNOWLEDGMENTS

This work was supported by the Center for Research in Human Movement Variability at the University of Nebraska at Omaha, funded by the NIH Award No. P20GM109090.

APPENDIX A: THEORETICAL MODELS

1. Fractional Brownian motion

In fractional Brownian motion (FBM), $x(t)$ is a Gaussian process with stationary increments; it is symmetric, $\langle x(t)\rangle = 0$, and importantly its EA-MSD scales as $\langle x(t)\rangle = 2K_H t^{2H}$, where H is the Hurst exponent and is related to the anomalous exponent α as $H = \alpha/2$ [53,192]. The two-time correlation for FBM is $\langle x(t_1)x(t_2)\rangle = K_H(t_1^{2H} + t_2^{2H} - |t_1 - t2|^{2H})$. FBM can also be defined as a process that arises from a generalized Langevin equation with nonwhite noise (or fractional Gaussian noise, fGn). The fGn has a standard normal distribution with zero mean and power-law correlations:

$$\langle \xi_{fGn}(t_1)\xi_{fGn}(t_2)\rangle = 2K_H H(2H-1)|t_1 - t2|^{2H-2} + 4K_H H|t_1 - t2|^{2H-1}\delta(t_1 - t2). \quad \text{(A1)}$$

The FBM features two regimes: one in which the noise is positively correlated ($1/2 < H < 1$, i.e., $1 < \alpha < 2$, superdiffusive) and the other in which the noise is negatively correlated ($0 < H < 2$, i.e., $0 < \alpha < 1$, subdiffusive). For $H = 1/2$ ($\alpha = 1$), the noise is uncorrelated. Hence the FBM converges to Brownian motion.

Various numerical approaches have been proposed to solve the FBM generalized Langevin equation. We use the method described by Bardet *et al.* [193] via the MATLAB function `wfbm()`. Details about the numerical implementations can be found in the associated reference.

2. Scaled Brownian motion

The scaled Brownian motion (SBM) is a process described by the Langevin equation with a time-dependent diffusivity

$$\frac{dx(t)}{dt} = \sqrt{2Kt}\xi(t), \quad \text{(A2)}$$

where $\xi = 1$ is white Gaussian noise [194]. In the case when $K(t)$ has a power-law dependence on t such that $K(t) = \alpha K_\alpha t^{\alpha-1}$, EA-MSD follows $\langle x^2(t)\rangle_N = K_\alpha t^\alpha$ with $K(t) = \Gamma(1+\alpha)K_\alpha$. The numerical implementation of SBM is presented in *Algorithm 1*.

Algorithm 1: Generate SBM trajectory

Input:
length of the trajectory T
anomalous exponent α
Define:
`erfcinv`$(\vec{a}) \rightarrow$ Inverse complementary error function of $\vec{a}$
U(L) $\rightarrow$ returns L uniform random numbers $\in [0, 1]$
Calculate:
$\vec{\Delta x} \leftarrow (1^\alpha, 2^\alpha, \ldots, T^\alpha) - (0^\alpha, 1^\alpha, \ldots, (T-1)^\alpha)$

$\vec{\Delta x} \leftarrow 2\sqrt{(2)}UL\vec{\Delta x}$
$\vec{x} \leftarrow$ cumsum $(\vec{\Delta x})$
Return: $\vec{x}$

3. Noisy continuous time random walk

The continuous time random walk (CTRW) is a family of random walks with arbitrary displacement density for which the waiting time, i.e., the time between subsequent steps, is a stochastic variable [57]. We considered a specific case of CTRW with waiting times following a power-law distribution $\psi(t) = t^{-\sigma}$ and displacements following a Gaussian distribution with variance D and zero means. In such case, the anomalous exponent is $\alpha = \sigma - 1$ [EA-MSD $= \langle x(t)^2 \rangle \propto t^{\alpha}$]. To obtain noisy CTRW (nCTRW) [56], white Gaussian noise with zero mean and standard deviation equal to the standard deviation of the corresponding CTRW fluctuation series was added to each CTRW series. Since the waiting times follow a power-law distribution, for $\sigma = 2$, EA-MSD features Brownian motion with logarithmic corrections [67].

The numerical implementation of CTRW is presented in **Algorithm 2**. Notice that the variable τ represents the total time at ith iteration. The output vector $\vec{x}$ corresponds to the position of the particle at the irregular times given by $\vec{t}$.

Algorithm 2: Generate CTRW trajectory

Input:
length of the trajectory T
anomalous exponent α
diffusion coefficient D
Define:
$\vec{x} \rightarrow$ empty vector
$\vec{t} \rightarrow$ empty vector
$N(\mu, S) \rightarrow$ Gaussian random number generator with mean μ and standard deviation $si = 0$; $\tau = 0$
While $\tau < T$ **do**
t_i sample randomly from $\psi(t) \sim t^{-\sigma}$
$x_i \leftarrow x_{i-1} + N(0, \sqrt{D})$
$\tau \leftarrow \tau + t_i$
$i \leftarrow i + 1$
end while
Return: $\vec{x}, \vec{t}$

4. Annealed transient time motion

The annealed transient time motion (ATTM) implements the motion of a Brownian particle with time-dependent diffusivity [58]. The observable performs Brownian motion for a random time t_1 with a random diffusion coefficient D_1, then for t_2 with D_2, and so on. The diffusion coefficients follow a distribution such that $P(D) = D^{\sigma-1}$ with $\sigma > 0$ as $D \rightarrow 0$, and that decays rapidly for large D. If the random times t are sampled from a distribution with expected value $E[t|D] = D^{-\gamma}$, with $\sigma < \gamma < \sigma + 1$, the anomalous exponent is $\alpha = \sigma/\gamma$. Here, we consider that the distribution is a δ function, $P_t(t|D) = \delta(1 - D^{-\gamma})$. Hence, the time t_i in which the observable performs Brownian motion with a random diffusion coefficient D_i is $t_i = D_i^{-\gamma}$, with D_i extracted from the distribution described above.

The numerical implementation of ATTM is presented in *Algorithm 3*. In contrast to nCTRW and LW, the only output is $\vec{x}$ because the trajectory is produced at regular intervals.

Algorithm 3: Generate ATTM trajectory

Input:
length of the trajectory T
anomalous exponent α
sampling time Δt
Define:
While $\sigma > \gamma$ and $\gamma > \sigma + 1$ **do**
$\sigma \leftarrow$ uniform random number $\in (0, 3]$
$\gamma = \sigma/\alpha$
end while
BM$(D, t, \Delta t) \rightarrow$ generates a Brownian motion trajectory of length t with diffusion coefficient D, sampled at time intervals Δt
While $\tau < T$ **do**
$D_i \leftarrow$ sample randomly from $P(D)D^{\sigma-1}$
$t_i \leftarrow D_i^{-\gamma}$
number of steps $N_i = round(t_i/\Delta t)$
$x_1, \ldots, x_{i+N_i} \leftarrow$ BM$(D, t, \Delta t)$
$i \leftarrow i + N_i + 1$
$\tau = \tau + N_i \Delta t$
end while
Return: $\vec{x}$

5. Lévy walk

The Lévy walk (LW) is a particular superdiffusive CTRW. Like subdiffusive CTRW, the flight time, i.e., the time between steps, for LW is irregular [59], but, in contrast to subdiffusive CTRW, the distribution of displacements for LW is not Gaussian. We considered the case in which the flight times follows the distribution $\psi(t) = t^{-\sigma-1}$. At each step, the displacement is Δx, and the step length is $|\Delta x|$. The displacements are correlated with the flight times such that the probability of moving a step Δx at time t and stopping at the new position to wait for a new random event to happen is $\psi(\Delta x, t) = \frac{1}{2}\delta(|\Delta x| - vt)\psi(t)$, where v is the velocity. The anomalous exponent is given by

$$\mathrm{EB}(x(t)) = \begin{cases} 2 & \text{if } 0 < \sigma < 1 \\ 3 - \sigma & \text{if } 1 < \sigma < 2. \end{cases} \tag{A3}$$

The numerical implementation of LW is presented in *Algorithm 4*. Notice that we use a random number r, which can take values 0 or 1, to decide in which sense the step is performed. The output vectors $\vec{x}$ represent irregularly sampled positions and times.

Algorithm 4: Generate LW trajectory

Input:
length of the trajectory T
anomalous exponent α
Define:
$\vec{x} \rightarrow$ empty vector
$\vec{t} \rightarrow$ empty vector
$v \rightarrow$ random number $\in (0, 10]$
$i = 0$
While $\tau < T$ **do**

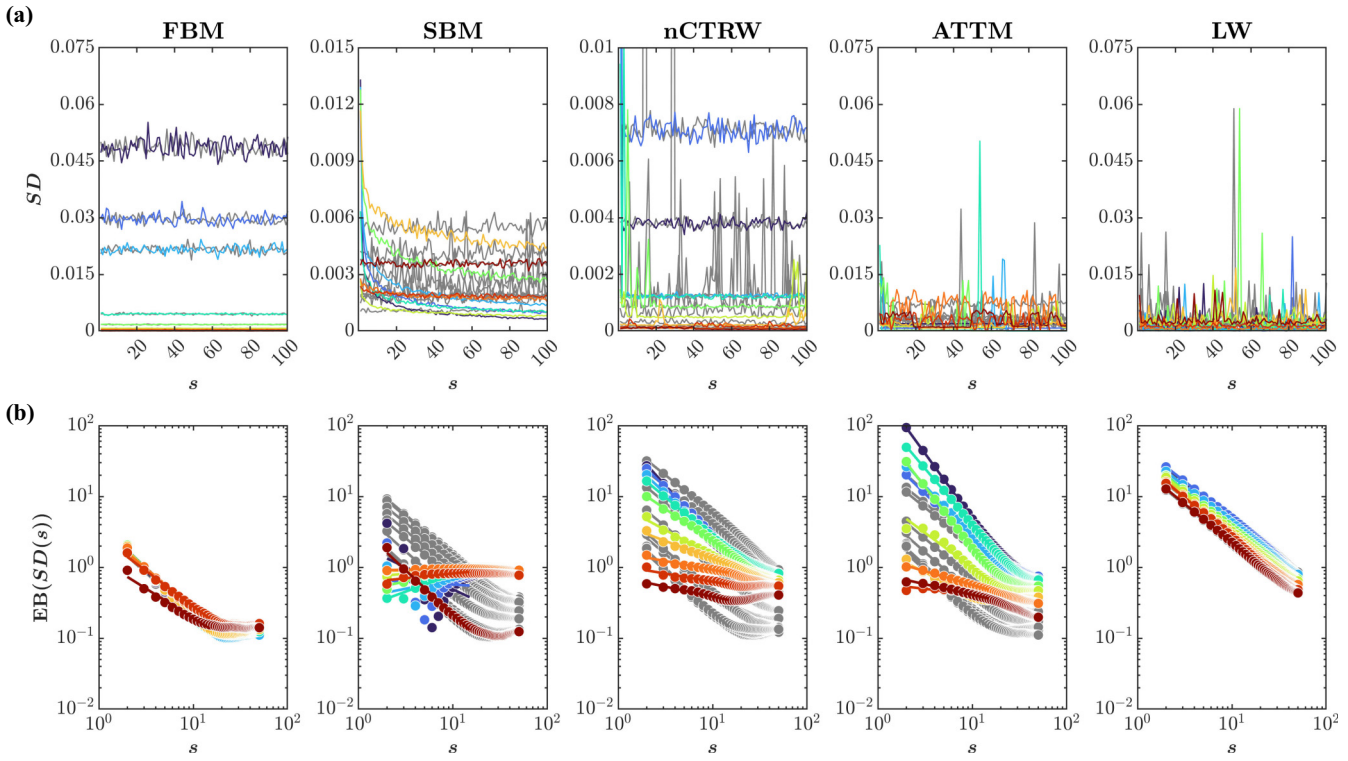

FIG. 8. Ergodicity breaking in *SD*. (a) Representative *SD* series (*SD* calculated across the 100 nonoverlapping 500-sample segments) for the five anomalous diffusion processes—FBM, SBM, nCTRW, ATTM, and LW. The anomalous exponent α ranges from 0.1 to 1 for FBM, SBM, nCTRW, and ATTM and from 1.1 to 2 for LW, with an increment of 0.1 from dark blue to dark red. Gray trajectories indicate *SD* series for the corresponding shuffled versions. (b) EB($SD(s)$) for the five processes and different values of α ($N = 100$; lag is $\Delta = 1$ segment). Gray curves indicate mean EB($SD(s)$) for the corresponding shuffled versions.

$t_i \leftarrow$ sample randomly from $\psi(t) \sim t_{-\sigma-1}$

$x_i(-1)^r v t_i$, where random r is 0 or 1 with equal probability.

$\tau \leftarrow \tau + t_i$

$i \leftarrow i + 1$

end while

Return: $\vec{x}, \vec{t}$

APPENDIX B: MSD-RELATED LINEAR DESCRIPTORS SUCH AS *SD*, *CV*, AND *RMS* REFLECT ERGODICITY-RELATED DIFFERENCES AMONG DIFFERENT ANOMALOUS DIFFUSION PROCESSES

SD for FBM for all values of the anomalous exponent α and SBM for $\alpha = 1$—the case in which SBM is reduced to awGn—return and converge towards the mean, suggestive of ergodicity [Fig. 8(a)]. In contrast, *SD* for SBM, nCTRW, ATTW, and LW diverge and never return towards the mean, suggesting ergodicity breaking in the *SD* series for these processes. The ergodicity-breaking parameter, i.e., EB($SD(s)$) confirmed these trends. EB $\rightarrow 0$ as $s \rightarrow \infty$ for FBM for all values of α and SBM for $\alpha = 1$—the case in which SBM is reduced to awGn [Fig. 8(b)]. EB shows no decay with s for SBM, a much slower decay with s for nCTRW, and a quick decay but to a much larger value for ATTM and LW, especially for larger values of α (i.e., $\alpha \rightarrow 1$), confirming ergodicity breaking in *SD* for these processes. Overall, the *SD* series for FBM, SBM, nCTRW, ATTM, and LW show highly variable initial rates of decay in EB: EB($SD(s)$) $= -1.32\frac{\Delta}{s}$ to $-0.84\frac{\Delta}{s}$, $-1.24\frac{\Delta}{s}$ to $0.49\frac{\Delta}{s}$, $-1.33\frac{\Delta}{s}$ to $-0.23\frac{\Delta}{s}$, $-1.70\frac{\Delta}{s}$ to $-0.30\frac{\Delta}{s}$, and $-1.12\frac{\Delta}{s}$ to $-1.04\frac{\Delta}{s}$, respectively, where $\Delta = 1$ (Table IV). In other words, the *SD* series for the five processes show highly variable decay rates in EB.

Except for some minor differences, the ergodicity-breaking behavior of *CV* resembles that of *SD*. *CV* for FBM return and

TABLE IV. The slopes of EB($SD(s)$) for the five anomalous diffusion processes and different values of α in terms of $\frac{\Delta}{s}$.

α[a]	FBM	SBM	cCTRW	ATTM	LW
0.1 (1.1)	−1.21	−0.62	−1.49	−1.83	−1.08
0.2 (1.2)	−1.26	−0.081	−1.33	−1.29	−1.04
0.3 (1.3)	−1.32	0.27	−1.26	−1.48	−1.04
0.4 (1.4)	−1.32	0.49	−1.12	−1.58	−1.08
0.5 (1.5)	−1.25	0.28	−0.90	−1.70	−1.04
0.6 (1.6)	−1.23	0.11	−0.72	−0.99	−1.09
0.7 (1.7)	−1.32	0.03	−0.50	−0.65	−1.08
0.8 (1.8)	−1.10	0.02	−0.25	−0.39	−1.10
0.9 (1.9)	−1.00	0.14	−0.23	−0.16	−1.12
1 (2)	−0.84	−1.24	−0.28	−0.30	−1.09

[a]The anomalous exponent α ranges from 0.1 to 1 for FBM, SBM, nCTRW, and ATTM and from 1.1 to 2 for LW (in parentheses).

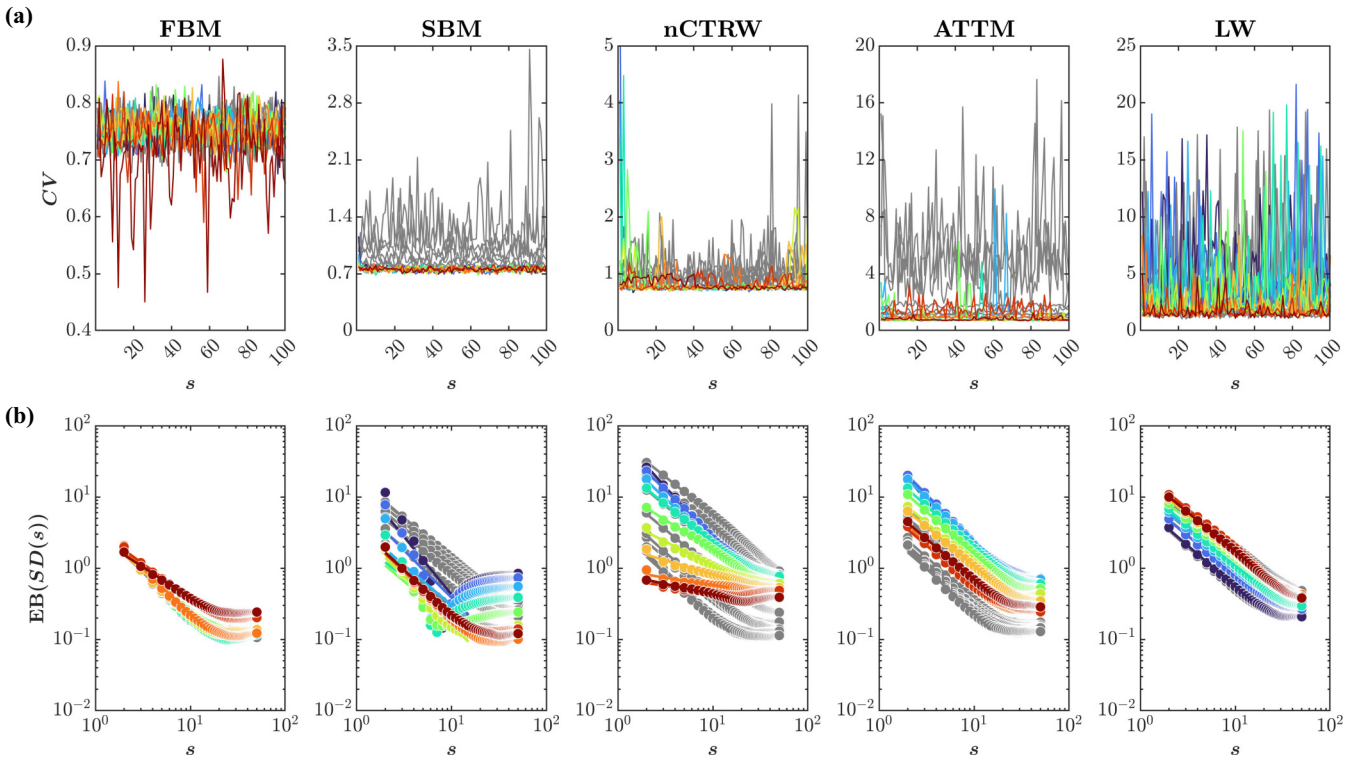

FIG. 9. Ergodicity breaking in CV. (a) Representative CV series (CV calculated across the 100 nonoverlapping 500-sample segments) for the five anomalous diffusion processes—FBM, SBM, nCTRW, ATTM, and LW. The anomalous exponent α ranges from 0.1 to 1 for FBM, SBM, nCTRW, and ATTM and from 1.1 to 2 for LW, with an increment of 0.1 from dark blue to dark red. Gray trajectories indicate CV series for the corresponding shuffled versions. (b) EB($CV(s)$) for the five processes and different values of α ($N = 100$; lag is $\Delta = 1$ segment). Gray curves indicate mean EB($CV(s)$) for the corresponding shuffled versions.

converge towards the mean for all values of the anomalous exponent α and SBM for $\alpha = 1$—the case in which SBM is reduced to awGn—return and converges towards the mean, suggestive of ergodicity [Fig. 9(a)]. In contrast, CV for SBM, nCTRW, ATTW, and LW diverge and never return towards the mean, suggesting ergodicity breaking in the CV series for these processes. EB($CV(s)$) confirmed these trends. EB $\to 0$ as $s \to \infty$ for FBM for the most part but show marginal ergodicity breaking for larger values of α [Fig. 9(b)]. CV series for SBM behaved ergodically for $\alpha = 1$—the case in which SBM is reduced to awGn, but CV series for SBM for other values of α showed strong ergodicity breaking. CV series for nCTRW break ergodicity, with stronger ergodicity breaking for larger α. CV series for ATTM and LW also show marginal ergodicity breaking, wherein EB quickly decayed with s but did not reach 1. Overall, the CV series for FBM, SBM, nCTRW, ATTM, and LW show highly variable initial rates of decay in EB: EB($CV(s)$) $= -1.33\frac{\Delta}{s}$ to $-0.87\frac{\Delta}{s}$, $-1.35\frac{\Delta}{s}$ to $-1.02\frac{\Delta}{s}$, $-1.33\frac{\Delta}{s}$ to $-0.29\frac{\Delta}{s}$, $-1.36\frac{\Delta}{s}$ to $-1.09\frac{\Delta}{s}$, and $-1.11\frac{\Delta}{s}$ to $-1.06\frac{\Delta}{s}$, respectively, where $\Delta = 1$

TABLE V. The slopes of EB($CV(s)$) for the five anomalous diffusion processes and different values of α in terms of $\frac{\Delta}{s}$.

α[a]	FBM	SBM	cCTRW	ATTM	LW
0.1 (1.1)	−1.26	−1.62	−1.49	−1.51	−1.15
0.2 (1.2)	−1.21	−1.33	−1.33	−1.36	−1.09
0.3 (1.3)	−1.27	−1.12	−1.26	−1.30	−1.10
0.4 (1.4)	−1.33	−1.02	−1.08	−1.19	−1.11
0.5 (1.5)	−1.22	−1.13	−0.84	−1.18	−1.06
0.6 (1.6)	−1.28	−1.35	−0.68	−1.13	−1.10
0.7 (1.7)	−1.20	−1.29	−0.39	−1.09	−1.09
0.8 (1.8)	−1.28	−1.33	−0.21	−1.20	−1.13
0.9 (1.9)	−0.96	−1.23	−0.21	−1.14	−1.10
1 (2)	−0.87	−1.24	−0.29	−1.13	−1.10

[a]The anomalous exponent α ranges from 0.1 to 1 for FBM, SBM, nCTRW, and ATTM and from 1.1 to 2 for LW (in parentheses).

TABLE VI. The slopes of EB($RMS(s)$) for the five anomalous diffusion processes and different values of α in terms of $\frac{\Delta}{s}$.

α[a]	FBM	SBM	cCTRW	ATTM	LW
0.1 (1.1)	−1.26	0.05	−1.49	−1.84	−1.08
0.2 (1.2)	−1.23	0.50	−1.33	−1.29	−1.04
0.3 (1.3)	−1.29	0.53	−1.26	−1.49	−1.04
0.4 (1.4)	−1.30	0.29	−1.12	−1.58	−1.08
0.5 (1.5)	−1.25	0.13	−0.91	−1.70	−1.04
0.6 (1.6)	−1.36	0.05	−0.74	−0.97	−1.09
0.7 (1.7)	−1.28	0.02	−0.54	−0.65	−1.08
0.8 (1.8)	−1.04	0.01	−0.27	−0.38	−1.10
0.9 (1.9)	−0.86	0.17	−0.25	−0.18	−1.12
1 (2)	−0.64	−1.28	−0.30	−0.32	−1.09

[a]The anomalous exponent α ranges from 0.1 to 1 for FBM, SBM, nCTRW, and ATTM and from 1.1 to 2 for LW (in parentheses).

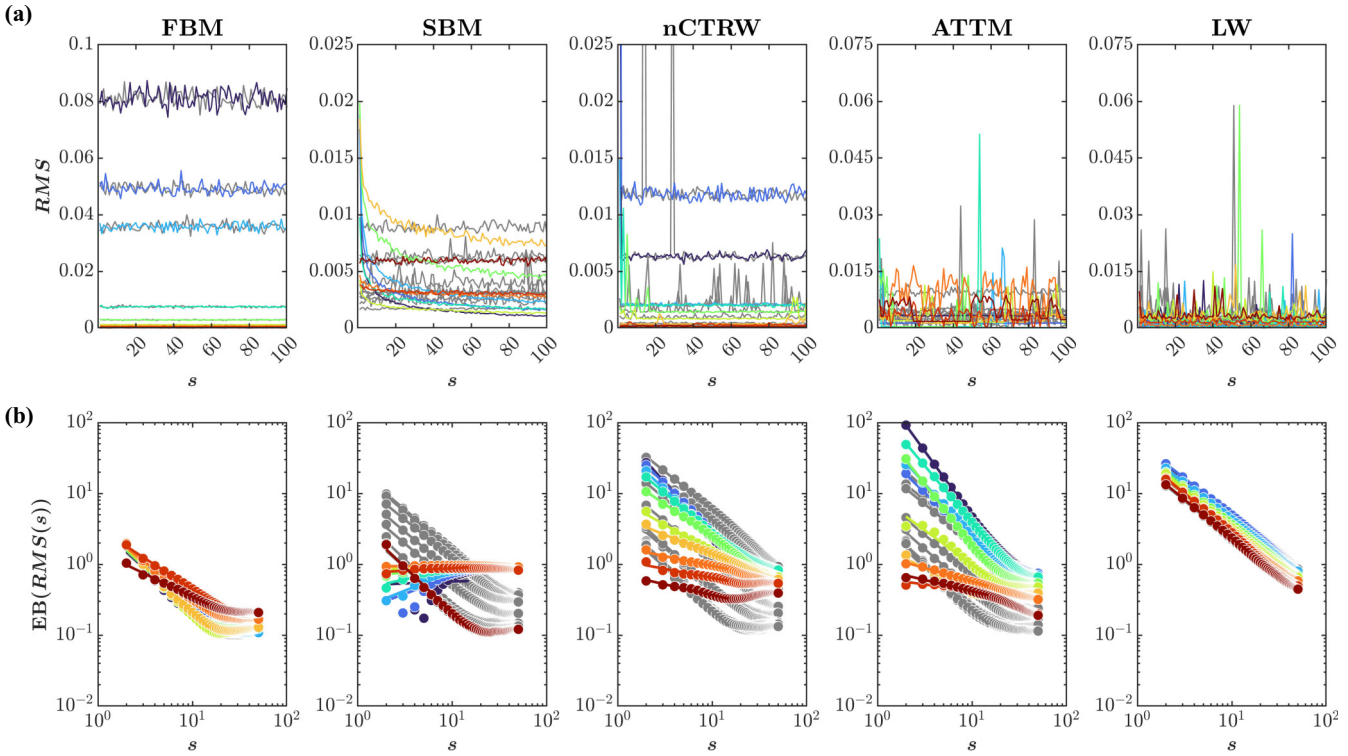

FIG. 10. Ergodicity breaking in *RMS*. (a) Representative *RMS* series (*RMS* calculated across the 100 nonoverlapping 500-sample segments) for the five anomalous diffusion processes—FBM, SBM, nCTRW, ATTM, and LW. The anomalous exponent α ranges from 0.1 to 1 for FBM, SBM, nCTRW, and ATTM and from 1.1 to 2 for LW, with an increment of 0.1 from dark blue to dark red. Gray trajectories indicate *RMS* series for the corresponding shuffled versions. (b) EB(*RMS*(*s*)) for the five processes and different values of α ($N = 100$; lag is $\Delta = 1$ segment). Gray curves indicate mean EB(*RMS*(*s*)) for the corresponding shuffled versions.

(Table V). In other words, the *CV* series for the five processes show highly variable decay rates in EB.

RMS series behaved exactly as *SD* series for all five processes. *RMS* for FBM for all values of the anomalous exponent α and SBM for $\alpha = 1$—the case in which SBM is reduced to awGn—return and converge towards the mean, suggestive of ergodicity [Fig. 10(a)]. In contrast, *RMS* for SBM, nCTRW, ATTW, and LW diverge and never return towards the mean, suggesting ergodicity breaking in the *RMS* series for these processes. EB(*RMS*(*s*)) confirmed these trends. EB $\to 0$ as $s \to \infty$ for FBM for all values of α and SBM for $\alpha = 1$—the case in which SBM is reduced to awGn [Fig. 10(b)]. EB shows no decay with s for SBM, a much slower decay with s for nCTRW, and a quick decay but to a much larger value for ATTM and LW, especially for larger values of α (i.e., $\alpha \to 1$), confirming ergodicity breaking in *RMS* for these processes. Overall, the *RMS* series for FBM, SBM, nCTRW, ATTM, and LW show highly variable initial rates of decay in EB(*RMS*(*s*)): EB(*RMS*(*s*)) $= -1.36\frac{\Delta}{s}$ to $-0.64\frac{\Delta}{s}$, $-1.28\frac{\Delta}{s}$ to $0.53\frac{\Delta}{s}$, $-0.25\frac{\Delta}{s}$ to $-1.49\frac{\Delta}{s}$, $-1.84\frac{\Delta}{s}$ to $-0.18\frac{\Delta}{s}$, and $-1.12\frac{\Delta}{s}$ to $-1.04\frac{\Delta}{s}$, respectively, where $\Delta = 1$ (Table VI). In other words, the *RMS* series for the five processes show highly variable decay rates in EB.

[1] Y. Sagi, M. Brook, I. Almog, and N. Davidson, Observation of Anomalous Diffusion and Fractional Self-Similarity in One Dimension, Phys. Rev. Lett. **108**, 093002 (2012).

[2] J. Zhao, Q. Deng, S. M. Avdoshenko, L. Fu, J. Eckert, and M. H. Rümmeli, Direct in situ observations of single Fe atom catalytic processes and anomalous diffusion at graphene edges, Proc. Natl. Acad. Sci. USA **111**, 15641 (2014).

[3] D. S. Banks and C. Fradin, Anomalous diffusion of proteins due to molecular crowding, Biophys. J. **89**, 2960 (2005).

[4] E. Barkai, Y. Garini, and R. Metzler, Strange kinetics of single molecules in living cells, Phys. Today **65**(8), 29 (2012).

[5] G. Guigas and M. Weiss, Sampling the cell with anomalous diffusion—The discovery of slowness, Biophys. J. **94**, 90 (2008).

[6] F. Höfling and T. Franosch, Anomalous transport in the crowded world of biological cells, Rep. Prog. Phys. **76**, 046602 (2013).

[7] J.-H. Jeon, V. Tejedor, S. Burov, E. Barkai, C. Selhuber-Unkel, K. Berg-Sørensen, L. Oddershede, and R. Metzler, *In Vivo* Anomalous Diffusion and Weak Ergodicity Breaking of Lipid Granules, Phys. Rev. Lett. **106**, 048103 (2011).

[8] J.-H. Jeon, H. M.-S. Monne, M. Javanainen, and R. Metzler, Anomalous Diffusion of Phospholipids and Cholesterols in a Lipid Bilayer and its Origins, Phys. Rev. Lett. **109**, 188103 (2012).

[9] D. Krapf and R. Metzler, Strange interfacial molecular dynamics, Phys. Today **72**(9), 48 (2019).

[10] R. Metzler and J. Klafter, The random walk's guide to anomalous diffusion: A fractional dynamics approach, Phys. Rep. **339**, 1 (2000).

[11] K. Ritchie, X.-Y. Shan, J. Kondo, K. Iwasawa, T. Fujiwara, and A. Kusumi, Detection of non-Brownian diffusion in the cell membrane in single molecule tracking, Biophys. J. **88**, 2266 (2005).

[12] I. M. Tolić-Nørrelykke, E.-L. Munteanu, G. Thon, L. Oddershede, and K. Berg-Sørensen, Anomalous Diffusion in Living Yeast Cells, Phys. Rev. Lett. **93**, 078102 (2004).

[13] T. E. Angelini, E. Hannezo, X. Trepat, M. Marquez, J. J. Fredberg, and D. A. Weitz, Glass-like dynamics of collective cell migration, Proc. Natl. Acad. Sci. USA **108**, 4714 (2011).

[14] P. Dieterich, R. Klages, R. Preuss, and A. Schwab, Anomalous dynamics of cell migration, Proc. Natl. Acad. Sci. USA **105**, 459 (2008).

[15] P. Dieterich, O. Lindemann, M. L. Moskopp, S. Tauzin, A. Huttenlocher, R. Klages, A. Chechkin, and A. Schwab, Anomalous diffusion and asymmetric tempering memory in neutrophil chemotaxis, PLoS Comput. Biol. **18**, e1010089 (2022).

[16] I. Golding and E. C. Cox, Physical Nature of Bacterial Cytoplasm, Phys. Rev. Lett. **96**, 098102 (2006).

[17] S. Hapca, J. W. Crawford, and I. M. Young, Anomalous diffusion of heterogeneous populations characterized by normal diffusion at the individual level, J. R. Soc., Interface **6**, 111 (2009).

[18] A. Lagarde, N. Dagès, T. Nemoto, V. Démery, D. Bartolo, and T. Gibaud, Colloidal transport in bacteria suspensions: From bacteria collision to anomalous and enhanced diffusion, Soft Matter **16**, 7503 (2020).

[19] S. Mukherjee, R. K. Singh, M. James, and S. S. Ray, Anomalous Diffusion and Lévy Walks Distinguish Active from Inertial Turbulence, Phys. Rev. Lett. **127**, 118001 (2021).

[20] S. Benhamou, How many animals really do the Lévy walk? Ecology **88**, 1962 (2007).

[21] A. James, M. J. Plank, and A. M. Edwards, Assessing Lévy walks as models of animal foraging, J. R. Soc., Interface **8**, 1233 (2011).

[22] A. M. Reynolds and C. J. Rhodes, The Lévy flight paradigm: Random search patterns and mechanisms, Ecology **90**, 877 (2009).

[23] C. T. Brown, L. S. Liebovitch, and R. Glendon, Lévy flights in Dobe Ju/'hoansi foraging patterns, Hum. Ecol. **35**, 129 (2007).

[24] D. A. Raichlen, B. M. Wood, A. D. Gordon, A. Z. Mabulla, F. W. Marlowe, and H. Pontzer, Evidence of Lévy walk foraging patterns in human hunter–gatherers, Proc. Natl. Acad. Sci. USA **111**, 728 (2014).

[25] A. G. Cherstvy, D. Vinod, E. Aghion, I. M. Sokolov, and R. Metzler, Scaled geometric Brownian motion features sub-or superexponential ensemble-averaged, but linear time-averaged mean-squared displacements, Phys. Rev. E **103**, 062127 (2021).

[26] V. Plerou, P. Gopikrishnan, L. A. N. Amaral, X. Gabaix, and H. E. Stanley, Economic fluctuations and anomalous diffusion, Phys. Rev. E **62**, R3023(R) (2000).

[27] A. Vázquez, J. G. Oliveira, Z. Dezsö, K.-I. Goh, I. Kondor, and A.-L. Barabási, Modeling bursts and heavy tails in human dynamics, Phys. Rev. E **73**, 036127 (2006).

[28] F. A. Oliveira, R. M. Ferreira, L. C. Lapas, and M. H. Vainstein, Anomalous diffusion: A basic mechanism for the evolution of inhomogeneous systems, Front. Phys. **7**, 18 (2019).

[29] I. M. Sokolov and J. Klafter, From diffusion to anomalous diffusion: A century after Einstein's Brownian motion, Chaos **15**, 026103 (2005).

[30] S. F. Timashev, Y. S. Polyakov, P. I. Misurkin, and S. G. Lakeev, Anomalous diffusion as a stochastic component in the dynamics of complex processes, Phys. Rev. E **81**, 041128 (2010).

[31] O. Vilk, E. Aghion, T. Avgar, C. Beta, O. Nagel, A. Sabri, R. Sarfati, D. K. Schwartz, M. Weiss, D. Krapf *et al.*, Unravelling the origins of anomalous diffusion: From molecules to migrating storks, Phys. Rev. Res. **4**, 033055 (2022).

[32] J. Dräger and J. Klafter, Strong Anomaly in Diffusion Generated by Iterated Maps, Phys. Rev. Lett. **84**, 5998 (2000).

[33] A. Godec, A. V. Chechkin, E. Barkai, H. Kantz, and R. Metzler, Localisation and universal fluctuations in ultraslow diffusion processes, J. Phys. A: Math. Theor. **47**, 492002 (2014).

[34] I. Goychuk, V. O. Kharchenko, and R. Metzler, Persistent Sinai-type diffusion in Gaussian random potentials with decaying spatial correlations, Phys. Rev. E **96**, 052134 (2017).

[35] A. Bancaud, S. Huet, N. Daigle, J. Mozziconacci, J. Beaudouin, and J. Ellenberg, Molecular crowding affects diffusion and binding of nuclear proteins in heterochromatin and reveals the fractal organization of chromatin, EMBO J. **28**, 3785 (2009).

[36] A. Caspi, R. Granek, and M. Elbaum, Enhanced Diffusion in Active Intracellular Transport, Phys. Rev. Lett. **85**, 5655 (2000).

[37] F. Höfling, K.-U. Bamberg, and T. Franosch, Anomalous transport resolved in space and time by fluorescence correlation spectroscopy, Soft Matter **7**, 1358 (2011).

[38] G. Seisenberger, M. U. Ried, T. Endress, H. Buning, M. Hallek, and C. Brauchle, Real-time single-molecule imaging of the infection pathway of an adeno-associated virus, Science **294**, 1929 (2001).

[39] P. R. Smith, I. E. Morrison, K. M. Wilson, N. Fernandez, and R. J. Cherry, Anomalous diffusion of major histocompatibility complex class I molecules on HeLa cells determined by single particle tracking, Biophys. J. **76**, 3331 (1999).

[40] S. C. Weber, A. J. Spakowitz, and J. A. Theriot, Bacterial Chromosomal Loci Move Subdiffusively through a Viscoelastic Cytoplasm, Phys. Rev. Lett. **104**, 238102 (2010).

[41] S. C. Weber, J. A. Theriot, and A. J. Spakowitz, Subdiffusive motion of a polymer composed of subdiffusive monomers, Phys. Rev. E **82**, 011913 (2010).

[42] D. Arcizet, B. Meier, E. Sackmann, J. O. Rädler, and D. Heinrich, Temporal Analysis of Active and Passive Transport in Living Cells, Phys. Rev. Lett. **101**, 248103 (2008).

[43] A. Caspi, R. Granek, and M. Elbaum, Diffusion and directed motion in cellular transport, Phys. Rev. E **66**, 011916 (2002).

[44] M. de Jager, F. J. Weissing, P. M. Herman, B. A. Nolet, and J. van de Koppel, Lévy walks evolve through interaction between movement and environmental complexity, Science **332**, 1551 (2011).

[45] M. H. G. Duits, Y. Li, S. A. Vanapalli, and F. Mugele, Mapping of spatiotemporal heterogeneous particle dynamics in living cells, Phys. Rev. E **79**, 051910 (2009).

[46] M. C. Gonzalez, C. A. Hidalgo, and A.-L. Barabasi, Understanding individual human mobility patterns, Nature (London) **453**, 779 (2008).

[47] F. Leoni and G. Franzese, Structural behavior and dynamics of an anomalous fluid between attractive and repulsive walls: Templating, molding, and superdiffusion, J. Chem. Phys. **141**, 174501 (2014).

[48] A. Mashanova, T. H. Oliver, and V. A. Jansen, Evidence for intermittency and a truncated power law from highly resolved aphid movement data, J. R. Soc., Interface **7**, 199 (2010).

[49] R. Nathan, W. M. Getz, E. Revilla, M. Holyoak, R. Kadmon, D. Saltz, and P. E. Smouse, A movement ecology paradigm for unifying organismal movement research, Proc. Natl. Acad. Sci. USA **105**, 19052 (2008).

[50] G. Muñoz-Gil, G. Volpe, M. A. Garcia-March, E. Aghion, A. Argun, C. B. Hong, T. Bland, S. Bo, J. A. Conejero, N. Firbas *et al.*, Objective comparison of methods to decode anomalous diffusion, Nat. Commun. **12**, 1 (2021).

[51] K. Pearson, The problem of the random walk, Nature (London) **72**, 294 (1905).

[52] J. Klafter and I. M. Sokolov, Anomalous diffusion spreads its wings, Phys. World **18**, 29 (2005).

[53] B. B. Mandelbrot and J. W. Van Ness, Fractional Brownian motions, fractional noises and applications, SIAM Rev. **10**, 422 (1968).

[54] S. C. Lim and S. V. Muniandy, Self-similar Gaussian processes for modeling anomalous diffusion, Phys. Rev. E **66**, 021114 (2002).

[55] J.-H. Jeon, A. V. Chechkin, and R. Metzler, Scaled Brownian motion: A paradoxical process with a time dependent diffusivity for the description of anomalous diffusion, Phys. Chem. Chem. Phys. **16**, 15811 (2014).

[56] J.-H. Jeon, E. Barkai, and R. Metzler, Noisy continuous time random walks, J. Chem. Phys. **139**, 121916 (2013).

[57] H. Scher and E. W. Montroll, Anomalous transit-time dispersion in amorphous solids, Phys. Rev. B **12**, 2455 (1975).

[58] P. Massignan, C. Manzo, J. A. Torreno-Pina, M. F. García-Parajo, M. Lewenstein, and G. J. Lapeyre, Jr, Nonergodic Subdiffusion from Brownian Motion in an Inhomogeneous Medium, Phys. Rev. Lett. **112**, 150603 (2014).

[59] J. Klafter and G. Zumofen, Lévy statistics in a Hamiltonian system, Phys. Rev. E **49**, 4873 (1994).

[60] J. Spiechowicz, I. G. Marchenko, P. Hänggi, and J. Łuczka, Diffusion coefficient of a Brownian particle in equilibrium and nonequilibrium: Einstein model and beyond, Entropy **25**, 42 (2023).

[61] Y. Lanoiselée and D. S. Grebenkov, Non-Gaussian diffusion of mixed origins, J. Phys. A: Math. Theor. **52**, 304001 (2019).

[62] D. S. Banks, C. Tressler, R. D. Peters, F. Höfling, and C. Fradin, Characterizing anomalous diffusion in crowded polymer solutions and gels over five decades in time with variable-lengthscale fluorescence correlation spectroscopy, Soft Matter **12**, 4190 (2016).

[63] J. A. Dix and A. Verkman, Crowding effects on diffusion in solutions and cells, Annu. Rev. Biophys. **37**, 247 (2008).

[64] D. Molina-Garcia, T. Sandev, H. Safdari, G. Pagnini, A. Chechkin, and R. Metzler, Crossover from anomalous to normal diffusion: Truncated power-law noise correlations and applications to dynamics in lipid bilayers, New J. Phys. **20**, 103027 (2018).

[65] I. M. Sokolov, Models of anomalous diffusion in crowded environments, Soft Matter **8**, 9043 (2012).

[66] S. Abe and S. Thurner, Anomalous diffusion in view of Einstein's 1905 theory of Brownian motion, Phys. A (Amsterdam, Neth.) **356**, 403 (2005).

[67] J. Klafter and I. M. Sokolov, *First Steps in Random Walks: From Tools to Applications* (Oxford University Press, Oxford, 2011).

[68] R. Metzler and J. Klafter, The restaurant at the end of the random walk: Recent developments in the description of anomalous transport by fractional dynamics, J. Phys. A: Math. Gen. **37**, R161 (2004).

[69] J. M. Sancho, A. M. Lacasta, K. Lindenberg, I. M. Sokolov, and A. H. Romero, Diffusion on a Solid Surface: Anomalous is Normal, Phys. Rev. Lett. **92**, 250601 (2004).

[70] I. M. Sokolov, J. Klafter, and A. Blumen, Fractional kinetics, Phys. Today **55**(11), 48 (2002).

[71] J. Krog and M. A. Lomholt, Bayesian inference with information content model check for Langevin equations, Phys. Rev. E **96**, 062106 (2017).

[72] J. Krog, L. H. Jacobsen, F. W. Lund, D. Wüstner, and M. A. Lomholt, Bayesian model selection with fractional Brownian motion, J. Stat. Mech.: Theory Exp. (2018) 093501.

[73] S. Park, S. Thapa, Y. Kim, M. A. Lomholt, and J.-H. Jeon, Bayesian inference of Lévy walks via hidden Markov models, J. Phys. A: Math. Theor. **54**, 484001 (2021).

[74] S. Thapa, M. A. Lomholt, J. Krog, A. G. Cherstvy, and R. Metzler, Bayesian analysis of single-particle tracking data using the nested-sampling algorithm: Maximum-likelihood model selection applied to stochastic-diffusivity data, Phys. Chem. Chem. Phys. **20**, 29018 (2018).

[75] S. Thapa, S. Park, Y. Kim, J.-H. Jeon, R. Metzler, and M. A. Lomholt, Bayesian inference of scaled versus fractional Brownian motion, J. Phys. A: Math. Theor. **55**, 194003 (2022).

[76] S. Bo, F. Schmidt, R. Eichhorn, and G. Volpe, Measurement of anomalous diffusion using recurrent neural networks, Phys. Rev. E **100**, 010102(R) (2019).

[77] F. Cichos, K. Gustavsson, B. Mehlig, and G. Volpe, Machine learning for active matter, Nat. Mach. Intell. **2**, 94 (2020).

[78] N. Granik, L. E. Weiss, E. Nehme, M. Levin, M. Chein, E. Perlson, Y. Roichman, and Y. Shechtman, Single-particle diffusion characterization by deep learning, Biophys. J. **117**, 185 (2019).

[79] J. Janczura, P. Kowalek, H. Loch-Olszewska, J. Szwabiński, and A. Weron, Classification of particle trajectories in living cells: Machine learning versus statistical testing hypothesis for fractional anomalous diffusion, Phys. Rev. E **102**, 032402 (2020).

[80] G. Muñoz-Gil, M. A. Garcia-March, C. Manzo, J. D. Martín-Guerrero, and M. Lewenstein, Single trajectory characterization via machine learning, New J. Phys. **22**, 013010 (2020).

[81] J. Pineda, B. Midtvedt, H. Bachimanchi, S. Noé, D. Midtvedt, G. Volpe, and C. Manzo, Geometric deep learning

reveals the spatiotemporal fingerprint of microscopic motion, arXiv:2202.06355.

[82] M. Gajowczyk, and J. Szwabiński, Detection of anomalous diffusion with deep residual networks, Entropy **23**, 649 (2021).

[83] A. Gentili and G. Volpe, Characterization of anomalous diffusion classical statistics powered by deep learning (condor), J. Phys. A: Math. Theor. **54**, 314003 (2021).

[84] P. Kowalek, H. Loch-Olszewska, Ł. Łaszczuk, J. Opała, and J. Szwabiński, Boosting the performance of anomalous diffusion classifiers with the proper choice of features, J. Phys. A: Math. Theor. **55**, 244005 (2022).

[85] G. Muñoz-Gil, G. G. i Corominas, and M. Lewenstein, Unsupervised learning of anomalous diffusion data an anomaly detection approach, J. Phys. A: Math. Theor. **54**, 504001 (2021).

[86] H. Seckler and R. Metzler, Bayesian deep learning for error estimation in the analysis of anomalous diffusion, Nat. Commun. **13**, 6717 (2022).

[87] P. Kowalek, H. Loch-Olszewska, and J. Szwabiński, Classification of diffusion modes in single-particle tracking data: Feature-based versus deep-learning approach, Phys. Rev. E **100**, 032410 (2019).

[88] H. Loch-Olszewska and J. Szwabiński, Impact of feature choice on machine learning classification of fractional anomalous diffusion, Entropy **22**, 1436 (2020).

[89] B. B. Mandelbrot, Intermittent turbulence in self-similar cascades: Divergence of high moments and dimension of the carrier, J. Fluid Mech. **62**, 331 (1974).

[90] D. Schertzer, S. Lovejoy, F. Schmitt, Y. Chigirinskaya, and D. Marsan, Multifractal cascade dynamics and turbulent intermittency, Fractals **05**, 427 (1997).

[91] N. Gal and D. Weihs, Experimental evidence of strong anomalous diffusion in living cells, Phys. Rev. E **81**, 020903(R) (2010).

[92] A. Rebenshtok and E. Barkai, Distribution of Time-Averaged Observables for Weak Ergodicity Breaking, Phys. Rev. Lett. **99**, 210601 (2007).

[93] M. F. Shlesinger, B. J. West, and J. Klafter, Lévy Dynamics of Enhanced Diffusion: Application to Turbulence, Phys. Rev. Lett. **58**, 1100 (1987).

[94] D. Ernst, J. Köhler, and M. Weiss, Probing the type of anomalous diffusion with single-particle tracking, Phys. Chem. Chem. Phys. **16**, 7686 (2014).

[95] Y. He, S. Burov, R. Metzler, and E. Barkai, Random Time-Scale Invariant Diffusion and Transport Coefficients, Phys. Rev. Lett. **101**, 058101 (2008).

[96] E. Kepten, A. Weron, G. Sikora, K. Burnecki, and Y. Garini, Guidelines for the fitting of anomalous diffusion mean square displacement graphs from single particle tracking experiments, PLoS One **10**, e0117722 (2015).

[97] D. Krapf, N. Lukat, E. Marinari, R. Metzler, G. Oshanin, C. Selhuber-Unkel, A. Squarcini, L. Stadler, M. Weiss, and X. Xu, Spectral Content of a Single Non-Brownian Trajectory, Phys. Rev. X **9**, 011019 (2019).

[98] M. Magdziarz, A. Weron, K. Burnecki, and J. Klafter, Fractional Brownian Motion Versus the Continuous-Time Random Walk: A Simple Test for Subdiffusive Dynamics, Phys. Rev. Lett. **103**, 180602 (2009).

[99] S. M. Rytov, Y. A. Kravtsov, and V. I. Tatarskii, *Principles of Statistical Radiophysics: Wave Propagation Through Random Media* (Springer, Berlin, 1989), Vol. 4.

[100] J. Ślęzak, R. Metzler, and M. Magdziarz, Codifference can detect ergodicity breaking and non-gaussianity, New J. Phys. **21**, 053008 (2019).

[101] V. Sposini, D. S. Grebenkov, R. Metzler, G. Oshanin, and F. Seno, Universal spectral features of different classes of random-diffusivity processes, New J. Phys. **22**, 063056 (2020).

[102] D. Thirumalai, R. D. Mountain, and T. R. Kirkpatrick, Ergodic behavior in supercooled liquids and in glasses, Phys. Rev. A **39**, 3563 (1989).

[103] O. Vilk, E. Aghion, R. Nathan, S. Toledo, R. Metzler, and M. Assaf, Classification of anomalous diffusion in animal movement data using power spectral analysis, J. Phys. A: Math. Theor. **55**, 334004 (2022).

[104] W. Deng and E. Barkai, Ergodic properties of fractional Brownian-Langevin motion, Phys. Rev. E **79**, 011112 (2009).

[105] D. G. Kelty-Stephen and M. Mangalam, Fractal and multifractal descriptors restore ergodicity broken by non-Gaussianity in time series, Chaos, Solitons Fractals **163**, 112568 (2022).

[106] D. G. Kelty-Stephen and M. Mangalam, Multifractal descriptors ergodically characterize non-ergodic multiplicative cascade processes, Phys. A (Amsterdam, Neth.) **617**, 128651 (2023).

[107] M. Mangalam and D. G. Kelty-Stephen, Point estimates, Simpson's paradox, and nonergodicity in biological sciences, Neurosci. Biobehav. Rev. **125**, 98 (2021).

[108] M. Mangalam and D. G. Kelty-Stephen, Ergodic descriptors of non-ergodic stochastic processes, J. R. Soc., Interface **19**, 20220095 (2022).

[109] M. Schwarzl, A. Godec, and R. Metzler, Quantifying non-ergodicity of anomalous diffusion with higher order moments, Sci. Rep. **7**, 3878 (2017).

[110] G. Bel and E. Barkai, Weak Ergodicity Breaking in the Continuous-Time Random Walk, Phys. Rev. Lett. **94**, 240602 (2005).

[111] S. Burov, J.-H. Jeon, R. Metzler, and E. Barkai, Single particle tracking in systems showing anomalous diffusion: The role of weak ergodicity breaking, Phys. Chem. Chem. Phys. **13**, 1800 (2011).

[112] A. G. Cherstvy and R. Metzler, Nonergodicity, fluctuations, and criticality in heterogeneous diffusion processes, Phys. Rev. E **90**, 012134 (2014).

[113] H. Safdari, A. G. Cherstvy, A. V. Chechkin, F. Thiel, I. M. Sokolov, and R. Metzler, Quantifying the non-ergodicity of scaled Brownian motion, J. Phys. A: Math. Theor. **48**, 375002 (2015).

[114] D. Froemberg and E. Barkai, Time-averaged Einstein relation and fluctuating diffusivities for the Lévy walk, Phys. Rev. E **87**, 030104(R) (2013).

[115] A. Godec and R. Metzler, Finite-Time Effects and Ultraweak Ergodicity Breaking in Superdiffusive Dynamics, Phys. Rev. Lett. **110**, 020603 (2013).

[116] J. A. Dixon, J. G. Holden, D. Mirman, and D. G. Stephen, Multifractal dynamics in the emergence of cognitive structure, Top. Cogn. Sci. **4**, 51 (2012).

[117] E. A. Ihlen and B. Vereijken, Interaction-dominant dynamics in human cognition: Beyond $1/f^{\alpha}$ fluctuation, J. Exp. Psychol.: Gen. **139**, 436 (2010).

[118] D. G. Kelty-Stephen, I. C. Lee, N. S. Carver, K. M. Newell, and M. Mangalam, Multifractal roots of suprapostural dexterity, Hum. Mov. Sci. **76**, 102771 (2021).

[119] H. Kloos and G. Van Orden, Voluntary behavior in cognitive and motor tasks, Mind and Matter **8**, 19 (2010).

[120] G. C. Van Orden, J. G. Holden, and M. T. Turvey, Self-organization of cognitive performance, J. Exp. Psychol.: Gen. **132**, 331 (2003).

[121] D. G. Kelty-Stephen, E. Lane, and M. Mangalam, Multifractal test for nonlinear changes in time series, Behav. Res. Methods (2021).

[122] M. Mangalam, N. S. Carver, and D. G. Kelty-Stephen, Multifractal signatures of perceptual processing on anatomical sleeves of the human body, J. R. Soc., Interface **17**, 20200328 (2020).

[123] C.-K. Peng, S. V. Buldyrev, S. Havlin, M. Simons, H. E. Stanley, and A. L. Goldberger, Mosaic organization of dna nucleotides, Phys. Rev. E **49**, 1685 (1994).

[124] C.-K. Peng, S. Havlin, H. E. Stanley, and A. L. Goldberger, Quantification of scaling exponents and crossover phenomena in nonstationary heartbeat time series, Chaos **5**, 82 (1995).

[125] A. Chhabra and R. V. Jensen, Direct Determination of the f(α) Singularity Spectrum, Phys. Rev. Lett. **62**, 1327 (1989).

[126] B. B. Mandelbrot and B. B. Mandelbrot, *The Fractal Geometry of Nature* (WH Freeman, New York, 1982), Vol. 1.

[127] T. C. Halsey, M. H. Jensen, L. P. Kadanoff, I. Procaccia, and B. I. Shraiman, Fractal measures and their singularities: The characterization of strange sets, Phys. Rev. A **33**, 1141 (1986).

[128] B. B. Mandelbrot, *Fractals and Scaling in Finance: Discontinuity, Concentration, Risk* (Springer, New York, 2013).

[129] M. Zamir, Critique of the test of multifractality as applied to biological data, J. Theor. Biol. **225**, 407 (2003).

[130] C. A. Bell, N. S. Carver, J. A. Zbaracki, and D. G. Kelty-Stephen, Non-linear amplification of variability through interaction across scales supports greater accuracy in manual aiming: Evidence from a multifractal analysis with comparisons to linear surrogates in the Fitts task, Front. Physiol. **10**, 998 (2019).

[131] L. Bloomfield, E. Lane, M. Mangalam, and D. G. Kelty-Stephen, Perceiving and remembering speech depend on multifractal nonlinearity in movements producing and exploring speech, J. R. Soc., Interface **18**, 20210272 (2021).

[132] N. S. Carver, D. Bojovic, and D. G. Kelty-Stephen, Multifractal foundations of visually-guided aiming and adaptation to prismatic perturbation, Hum. Mov. Sci. **55**, 61 (2017).

[133] N. S. Carver and D. G. Kelty-Stephen, Multifractality in individual honeybee behavior hints at colony-specific social cascades: Reanalysis of radio-frequency identification data from five different colonies, Phys. Rev. E **95**, 022402 (2017).

[134] N. Jacobson, Q. Berleman-Paul, M. Mangalam, D. G. Kelty-Stephen, and C. Ralston, Multifractality in postural sway supports quiet eye training in aiming tasks: A study of golf putting, Hum. Mov. Sci. **76**, 102752 (2021).

[135] D. G. Kelty-Stephen, L. A. Stirling, and L. A. Lipsitz, Multifractal temporal correlations in circle-tracing behaviors are associated with the executive function of rule-switching assessed by the Trail Making Test, Psychol. Assess. **28**, 171 (2016).

[136] D. G. Kelty-Stephen, M. P. Furmanek, and M. Mangalam, Multifractality distinguishes reactive from proactive cascades in postural control, Chaos, Solitons Fractals **142**, 110471 (2021).

[137] M. Mangalam and D. G. Kelty-Stephen, Multiplicative-cascade dynamics supports whole-body coordination for perception via effortful touch, Hum. Mov. Sci. **70**, 102595 (2020).

[138] D. G. Stephen and J. A. Dixon, Strong anticipation: Multifractal cascade dynamics modulate scaling in synchronization behaviors, Chaos, Solitons Fractals **44**, 160 (2011).

[139] D. G. Stephen, W.-H. Hsu, D. Young, E. L. Saltzman, K. G. Holt, D. J. Newman, M. Weinberg, R. J. Wood, R. Nagpal, and E. C. Goldfield, Multifractal fluctuations in joint angles during infant spontaneous kicking reveal multiplicativity-driven coordination, Chaos, Solitons Fractals **45**, 1201 (2012).

[140] D. W. Teng, C. L. Eddy, and D. G. Kelty-Stephen, Non-visually-guided distance perception depends on matching torso fluctuations between training and test, Atten. Percept. Psychophys. **78**, 2320 (2016).

[141] R. M. Ward and D. G. Kelty-Stephen, Bringing the nonlinearity of the movement system to gestural theories of language use: Multifractal structure of spoken English supports the compensation for coarticulation in human speech perception, Front. Physiol. **9**, 1152 (2018).

[142] E. A. F. E. Ihlen, Introduction to multifractal detrended fluctuation analysis in Matlab, Front. Physiol. **3**, 141 (2012).

[143] T. Schreiber and A. Schmitz, Improved Surrogate Data for Nonlinearity Tests, Phys. Rev. Lett. **77**, 635 (1996).

[144] A. G. Cherstvy, A. V. Chechkin, and R. Metzler, Anomalous diffusion and ergodicity breaking in heterogeneous diffusion processes, New J. Phys. **15**, 083039 (2013).

[145] R. Metzler, J.-H. Jeon, A. G. Cherstvy, and E. Barkai, Anomalous diffusion models and their properties: Non-stationarity, non-ergodicity, and ageing at the centenary of single particle tracking, Phys. Chem. Chem. Phys. **16**, 24128 (2014).

[146] F. Thiel and I. M. Sokolov, Scaled Brownian motion as a mean-field model for continuous-time random walks, Phys. Rev. E **89**, 012115 (2014).

[147] J.-H. Jeon and R. Metzler, Analysis of short subdiffusive time series: Scatter of the time-averaged mean-squared displacement, J. Phys. A: Math. Theor. **43**, 252001 (2010).

[148] D. G. Kelty-Stephen, K. Palatinus, E. Saltzman, and J. A. Dixon, A tutorial on multifractality, cascades, and interactivity for empirical time series in ecological science, Ecol. Psychol. **25**, 1 (2013).

[149] S. Ritschel, A. G. Cherstvy, and R. Metzler, Universality of delay-time averages for financial time series: Analytical results, computer simulations, and analysis of historical stock-market prices, J. Phys.: Complex. **2**, 045003 (2021).

[150] D. Vinod, A. G. Cherstvy, W. Wang, R. Metzler, and I. M. Sokolov, Nonergodicity of reset geometric Brownian motion, Phys. Rev. E **105**, L012106 (2022).

[151] W. Wang, A. G. Cherstvy, R. Metzler, and I. M. Sokolov, Restoring ergodicity of stochastically reset anomalous-diffusion processes, Phys. Rev. Res. **4**, 013161 (2022).

[152] S. Kian-Bostanabad and M.-R. Azghani, The relationship between rms electromyography and thickness change in the skeletal muscles, Med. Eng. Phys. **43**, 92 (2017).

[153] J. Vink, M. Westover, A. Pascual-Leone, and M. Shafi, Eeg functional connectivity predicts propagation of tms-evoked potentials, Brain Stimul. **10**, 516 (2017).

[154] J. J. Vink, D. C. Klooster, R. A. Ozdemir, M. B. Westover, A. Pascual-Leone, and M. M. Shafi, Eeg functional connectivity is a weak predictor of causal brain interactions, Brain Topogr. **33**, 221 (2020).

[155] C. R. Booth, H. L. Brown, E. G. Eason, S. Wallot, and D. G. Kelty-Stephen, Expectations on hierarchical scales of discourse: Multifractality predicts both short-and long-range effects of violating gender expectations in text reading, Discourse Process. **55**, 12 (2018).

[156] D. G. Kelty-Stephen and J. A. Dixon, Interwoven fluctuations during intermodal perception: Fractality in head sway supports the use of visual feedback in haptic perceptual judgments by manual wielding, J. Exp. Psychol. Hum. Percept. Perform. **40**, 2289 (2014).

[157] M. Mangalam, R. Chen, T. R. McHugh, T. Singh, and D. G. Kelty-Stephen, Bodywide fluctuations support manual exploration: Fractal fluctuations in posture predict perception of heaviness and length via effortful touch by the hand, Hum. Mov. Sci. **69**, 102543 (2020).

[158] M. Mangalam, N. S. Carver, and D. G. Kelty-Stephen, Global broadcasting of local fractal fluctuations in a bodywide distributed system supports perception via effortful touch, Chaos, Solitons Fractals **135**, 109740 (2020).

[159] S. Wallot and D. G. Kelty-Stephen, Interaction-dominant causation in mind and brain, and its implication for questions of generalization and replication, Mines Mach. **28**, 353 (2018).

[160] N. Cardenas, S. Kumar, and S. Mohanty, Dynamics of cellular response to hypotonic stimulation revealed by quantitative phase microscopy and multi-fractal detrended fluctuation analysis, Appl. Phys. Lett. **101**, 203702 (2012).

[161] S. Chaieb, Š. Málková, and J. Lal, Why the wrinkling transition in partially polymerized membranes is not universal? Fractal-multifractal hierarchy, J. Theor. Biol. **251**, 60 (2008).

[162] V. Rezania, F. C. Sudirga, and J. A. Tuszynski, Multifractality nature of microtubule dynamic instability process, Phys. A (Amsterdam, Neth.) **573**, 125929 (2021).

[163] A. Wawrzkiewicz-Jałowiecka, P. Trybek, B. Dworakowska, and Ł. Machura, Multifractal properties of BK channel currents in human glioblastoma cells, J. Phys. Chem. B **124**, 2382 (2020).

[164] E. D. Gutiérrez and J. L. Cabrera, A neural coding scheme reproducing foraging trajectories, Sci. Rep. **5**, 1 (2015).

[165] Y. Ikeda, P. Jurica, H. Kimura, H. Takagi, Z. R. Struzik, K. Kiyono, Y. Arata, and Y. Sako, C. elegans episodic swimming is driven by multifractal kinetics, Sci. Rep. **10**, 1 (2020).

[166] F. G. Schmitt and L. Seuront, Multifractal random walk in copepod behavior, Phys. A (Amsterdam, Neth.) **301**, 375 (2001).

[167] L. Seuront and H. E. Stanley, Anomalous diffusion and multifractality enhance mating encounters in the ocean, Proc. Natl. Acad. Sci. USA **111**, 2206 (2014).

[168] V. Balaban, S. Lim, G. Gupta, J. Boedicker, and P. Bogdan, Quantifying emergence and self-organisation of *enterobacter cloacae* microbial communities, Sci. Rep. **8**, 12416 (2018).

[169] H. Koorehdavoudi, P. Bogdan, G. Wei, R. Marculescu, J. Zhuang, R. W. Carlsen, and M. Sitti, Multi-fractal characterization of bacterial swimming dynamics: A case study on real and simulated *Serratia marcescens*, Proc. R. Soc. London, Ser. A **473**, 20170154 (2017).

[170] Y. Chen, M. Ding, and J. A. S. Kelso, Long Memory Processes ($1/f^{\alpha}$ Type) in Human Coordination, Phys. Rev. Lett. **79**, 4501 (1997).

[171] A. B. Slifkin and J. R. Eder, Trajectory evolution and changes in the structure of movement amplitude time series, Hum. Mov. Sci. **71**, 102617 (2020).

[172] S. Lovejoy and D. Schertzer, *The Weather and Climate: Emergent Laws and Multifractal Cascades* (Cambridge University Press, Cambridge, 2018).

[173] L. R. Karhausen, Commentary: Coda—a socratic dialogue: Plato, Int. J. Epidemiol. **30**, 710 (2001).

[174] R. Bahar, C. H. Hartmann, K. A. Rodriguez, A. D. Denny, R. A. Busuttil, M. E. Dollé, R. B. Calder, G. B. Chisholm, B. H. Pollock, C. A. Klein *et al.*, Increased cell-to-cell variation in gene expression in ageing mouse heart, Nature (London) **441**, 1011 (2006).

[175] F. Sanabria, Internal-clock models and misguided views of mechanistic explanations: A reply to Eckard & Lattal (2020), Perspect. Behav. Sci. **43**, 779 (2020).

[176] E. Shahar, Estimating causal parameters without target populations, J. Eval. Clin. Pract. **13**, 814 (2007).

[177] J. Vijg, Loss of gene coordination as a stochastic cause of ageing, Nat. Metab. **2**, 1188 (2020).

[178] J. van Hateren, Active causation and the origin of meaning, Biol. Cybern. **109**, 33 (2015).

[179] O. M. Cliff, J. T. Lizier, N. Tsuchiya, and B. D. Fulcher, Unifying pairwise interactions in complex dynamics, arXiv:2201.11941.

[180] B. D. Fulcher, M. A. Little, and N. S. Jones, Highly comparative time-series analysis: The empirical structure of time series and their methods, J. R. Soc., Interface **10**, 20130048 (2013).

[181] B. D. Fulcher and N. S. Jones, Hctsa: A computational framework for automated time-series phenotyping using massive feature extraction, Cell Syst. **5**, 527 (2017).

[182] S. Lovejoy, D. Schertzer, and P. Silas, Diffusion in one-dimensional multifractal porous media, Water Resour. Res. **34**, 3283 (1998).

[183] V. V. Afanasiev, R. Z. Sagdeev, and G. M. Zaslavsky, Chaotic jets with multifractal space-time random walk, Chaos **1**, 143 (1991).

[184] W. Chen, H. Sun, X. Zhang, and D. Korošak, Anomalous diffusion modeling by fractal and fractional derivatives, Comput. Math. Appl. **59**, 1754 (2010).

[185] J.-R. de Dreuzy, P. Davy, J. Erhel, and J. de Brémond d'Ars, Anomalous diffusion exponents in continuous two-dimensional multifractal media, Phys. Rev. E **70**, 016306 (2004).

[186] L. Gmachowski, Fractal model of anomalous diffusion, Eur. Biophys. J. **44**, 613 (2015).

[187] D. R. Bickel, Simple estimation of intermittency in multifractal stochastic processes: Biomedical applications, Phys. Lett. A **262**, 251 (1999).

[188] R. Menu and T. Roscilde, Anomalous Diffusion and Localization in a Positionally Disordered Quantum Spin Array, Phys. Rev. Lett. **124**, 130604 (2020).

[189] L. Seuront, F. G. Schmitt, M. C. Brewer, J. R. Strickler, and S. Souissi, From random walk to multifractal random walk in zooplankton swimming behavior, Zool. Stud. **43**, 498 (2004).

[190] A. Sharifi-Viand, M. Mahjani, and M. Jafarian, Investigation of anomalous diffusion and multifractal dimensions in polypyrrole film, J. Electroanal. Chem. **671**, 51 (2012).

[191] M. R. Shaebani, A. Wysocki, R. G. Winkler, G. Gompper, and H. Rieger, Computational models for active matter, Nat. Rev. Phys. **2**, 181 (2020).

[192] J.-H. Jeon and R. Metzler, Fractional Brownian motion and motion governed by the fractional Langevin equation in confined geometries, Phys. Rev. E **81**, 021103 (2010).

[193] J.-M. Bardet, G. Lang, G. Oppenheim, A. Philippe, and M. S. Taqqu, Generators of long-range dependent processes: A survey, in *Theory and Applications of Long-Range Dependence*, edited by P. Doukhan, G. Oppenheim, and M. A. Taqqu (Birkhäuser, Boston, 2003), pp. 579–623.

[194] G. Muñoz-Gil, C. Romero-Aristizabal, N. Mateos, F. Campelo, L. I. de Llobet Cucalon, M. Beato, M. Lewenstein, M. F. Garcia-Parajo, and J. A. Torreno-Pina, Stochastic particle unbinding modulates growth dynamics and size of transcription factor condensates in living cells, Proc. Natl. Acad. Sci. USA **119**, e2200667119 (2022).